Combined Nanochannel-Nanopore Device for Single-Molecule DNA Analysis and Manipulation

Yuning Zhang

Master of Science

Department of Physics

McGill University

Montreal,Quebec

May 02,2012

A Thesis Submitted to the Faculty of Graduate Studies in partial fulfillment of the requirements for the degree of Master of Science

ACKNOWLEDGEMENTS

This work would not have been possible without the encouragement and generous help from many people. First and foremost, I would like to thank my supervisor Walter Reisner. His careful instruction and acute intuitive insight into physics guided me through this project. I would like to thank David Laleyan, who assisted me in finishing the standard nanopore experiment during the summer of 2011. I would also like to thank the other members of the Reisner group, Ilja Czolkos, Alexander Klotz, Robert Welch, Ahmed Khorshid and Yi Cao, for providing me invaluable help during experiments. I am enormously indebted to the McGill Nanotools staffs, who provided me systematic training on the micro/nanofabrication tools. I also deeply appreciate Jean-Philippe Masse and Guillaume Dauphinais, who trained me on transmission electron microscope and nanopore fabrication. Sincere thanks to Mathieu Cesar for helping me translate the abstract into French.

Lastly, I wish to thank my parents and all of my friends, from whom I received enormous support, both physically and spiritually. To them I dedicate this thesis.

ABSTRACT

Nanofluidic devices, containing features with dimensions of 1-100 nm, allow for the direct detection, analysis and manipulation of single molecule analytes. In particular, over the past ten years, there has been increasing interest in developing nanofluidic devices capable of analyzing DNA at the single-molecule level, with the goal of developing high throughput mapping and eventually sequencing technology. Part of this thesis will be focusing on single-molecular DNA detection using solid state nanopores. The nanopore fabrication technique via electron beam ablation will be presented. Noise reduction is affected by coating a layer of PDMS(polydimethylsiloxane) on the nanopore supporting chip. Different folding states of DNA molecules translocating through the nanopore are observed.

Since the classic nanopore setup has low signal to noise ratio, we have successfully fabricated a novel micro/nanoiudic device combining nanopore detectors with nanochannels devices by embedding a nanopore inside the nanochannel. The device concept, device fabrication, theoretical analysis and preliminary results will be covered in this thesis.

ABRÉGÉ

Les dispositifs nanofluides, dont certaines parties atteignent des dimensions de l'ordre de 1-100 nm, permettent la dtection directe, l'analyse et la manipulation d'analyte molcule unique. En particulier, durant les dernires dix annes, il y a eu un intrt croissant au dveloppement de dispositifs nanofluides capables d'analyser de l'ADN au niveau des molcules individuelles, avec pour but le dveloppement d'une technologie de cartographie et ventuellement de squenage haut dbit. Une partie de ce mmoire se concentrera sur la dtection d'ADN molcule unique en utilisant des nanopores solides.

La technique de fabrication de nanopores via ablation par faisceau d'lectrons sera prsente. La rduction de bruit est affecte par le dpt d'une couche de PDMS (poly-dimthylsiloxane) sur la puce supportant le nanopore. Diffrentes conformations des molcules d'ADN se dplaant travers le nanopore sont observes. Puisque le montage classique du nanopore a un faible rapport signal-bruit, nous avons russi fabriquer un nouveau dispositif micro/nanofluide combinant des nanopores dtecteurs avec des nanoconduits en intgrant un nanopore dans le nanoconduit. La conception du dispositif, sa fabrication, l'analyse thorique et des rsultats prliminaires seront couverts dans ce mmoire.

TABLE OF CONTENTS

LIST OF TABLES

LIST OF FIGURES

CHAPTER 1
Introduction

1.1 DNA

Deoxyribonucleic acid (DNA) is a long polymer chain of repeating units called nucleotides, consisting of backbones made of sugars and phosphate groups joined by phosphodiester bonds. In the double stranded helix structure, backbones that belong to different chains are joined together by hydrogen-bonded nucleobases. DNA contains four types of nucleobases: adenine (T), guanine (G), cytosine (C), and thymine (T). In canoncial Watson-Crick base-pairing, A pairs with T and G pairs with C, the basis for how genetic information is propagated via semiconservative replication. The double ringed-bases such as G and A, the 'purines' can only pair with single-ring bases, the 'pyrimidines' (C and T). The mis-matched pairings (AC, GT) are unfavorable as there is a mis-match between the number of hydrogen bond donors and acceptors (GC pairings have three hyrogen bonds; AT pairings have two). The sequence of the nucleobases encodes the genetic information of the organism. While in cells, DNA strands are complexed with proteins into highly condensed structures called chromosomes. The complete sequence of an organism (the organism's "genome"), contains regions that code for all proteins ('genes'), microRNA's, transfer/ribosomal RNA and regions of unknown function/significance ('junk' DNA).

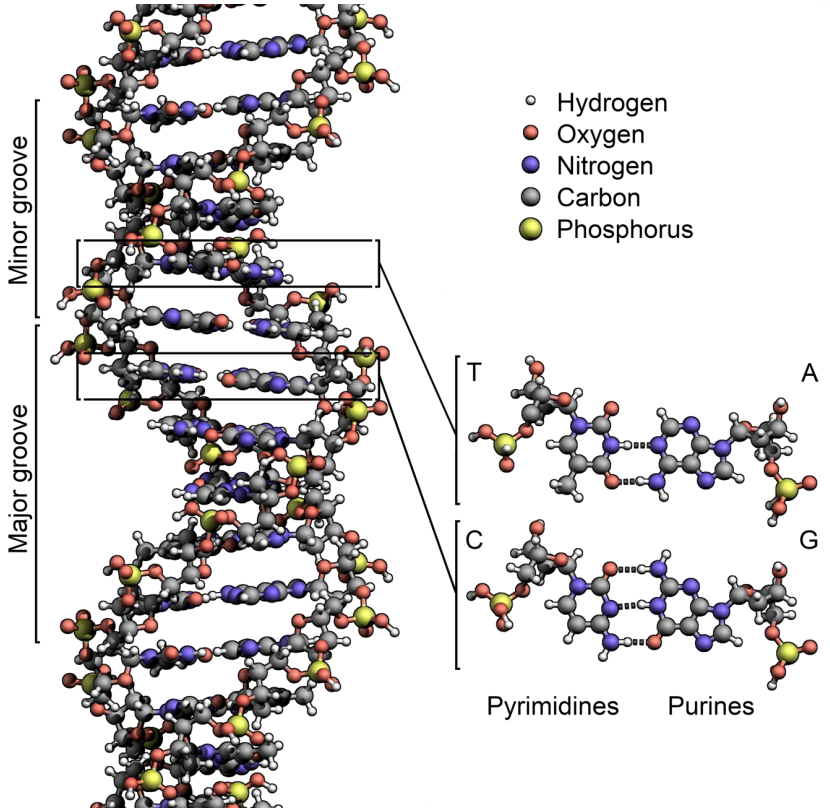

Figure 1–1: The double helix structure of DNA molecule. (Image from Wikipedia, term: DNA.)

1.2 DNA sequencing technology

The blueprint of each living organism is encoded in that organism's DNA sequence. Determining the the order of the nucleotide bases is therefore foundational for biological research. Sequence information is critical for routine diagnosis of genetic diseases. In the near future, there is hope as well that inexpensive sequencing technology will allow for personalized treatment plans(e.g. sequencing the genome of cells drawn from a particular tumor to assess the tumor's susceptibility to a given therapy).

During the 1970s, Allan Maxam and Walter Gillbert developed one of the earliest DNA sequencing techniques based on chemical modification of DNA using the "wandering-spot analysis" [1]. In 1977, Frederick Sanger developed the chain-termination method using dideoxynucleotide triphosphates (ddNTPs) as DNA chain terminators [2]. With this technique, researchers have successfully sequenced the phage genome and most of the human genome for the human genome project (HGP) via factories housing multiple capillary electrophoresis sequencer platforms. However, the expensive cost as well as the low throughput drives researchers to develop the second generation sequencing technique. In the beginning of 21st century, the development of 454 pyrosequencing, Illumina (Solexa) sequencing and SOLiD sequencing is a milestone of developing second generation high-throughput automated sequencing technologies. However the eager for single molecular sequencing as well as further lowering costs, initiated by the goal of the NIH 'thousand-dollar genome' [3, 4] project, led to the development of third generation DNA sequencing. New sequencing techniques that extended sequencing length also at a lower cost, such as the Helioscope(TM) single molecule sequencing, single molecule SMRT(TM) sequencing, single molecule real time (RNAP) sequencing and nanopore DNA sequencing, are developed.

1.3 Nanopore sensors

The idea of using nanopores as sensors for DNA was proposed in the 1990s [5]. When DNA passes through a sub 10 nm pore in a thin membrane (<50 nm), under the influence of an applied electric field, the presence of the molecule in the pore will physically block the passage of ions, creating a distinct electrical "blockade" in the trans-pore current. The concept of nanopore sequencing is that when DNA molecule translocate through a nanoscale pore in a linear conformation,

the passage of each base through the pore will create a distinct base-specific modulation in the signal, so that the sequence can be read off of the structure of the translocation current blockade [5]. The first experimental results were reported in 1996 by John Kasianowicz using a biological pore α-haemolysin (αHL) [6]. The α-haemolysin is formed by inserting a single protein nanopore into a lipid bilayer membrane and has a total length of $\sim 10\,\mathrm{nm}$. During these experiments, Kasianowicz found that the α-hemolysin pore remains open at neutral pH and high ionic strength and it passes a steady ionic current in the range of 100 picoamperes (pA) when applied a voltage of 100 mV [5]. Because of these features, α-hemolysin pores are intensively used in the nanopore field.

Even though bio-pores have proved to work well as functioning nanopore detectors for polymer translocation experiments, they have many disadvantages: the inability of changing pore size due to the fixed-structure; limited stability determined by the environment parameters such as pH, salt concentration and temperature. However, the solid state nanopores which are generally fabricated in silicon compound membranes, have the features of high stability, tunable size, adjustable surface properties and the potential for integration into devices [7]. Solid state nanopores can be made via various techniques including ion-beam sculpting [8] and electron beams [9], which will be introduced in chapter 2.

A simple Ag/AgCl electrode system is used for the classic nanopore experiment. As shown in figure 1-2, a voltage is applied across the Ag/AgCl electrodes, which are dipped into the conductive solution, creating a strong electric field ($\sim 10^6\,V/m$) across the pore region. The electric field subsequently drives a flow of ions through the nanopore, creating a stable trans-pore current. DNA itself is also negatively charged (charge density two electron per base pair) because of

the negative phosphate ions in the backbone. Thus DNA molecules will also be driven through the nanopore via potential. When DNA molecules pass through the pore, they block the ionic flow, creating a transient dip (blockade) in the trans-pore current flow. Because of the nanopore has a diameter comparable to the DNA molecular width ($\sim 2.5\,\mathrm{nm}$), DNA conformation–length, folding and untimately sequence information–can be determined by analysing the duration and magnitude these blockades.

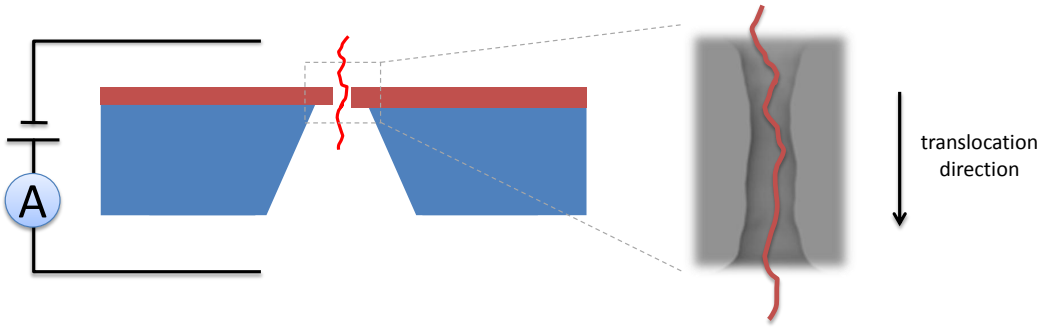

Figure 1–2: Nanopore-based DNA analysis. Voltage applied to the electrolytic solution (e.g. KCl) through Ag/AgCl electrodes drives a flow of ions (K^+, Cl^-) through the nanopore. Negatively charged DNA molecules are also driven through the pore, blocking the ions, creating a transient dip in the trans-current trace.

However, the classic nanopore setup has two key disadvantages: 1. DNA molecule translocate rapidly (1 to $5\,\mu$s per base) through the nanopore, fail to provide single-nucleotide resolution in the electric measurements; 2. there exists an unfavorable tradeoff between translocation speed and signal. Increasing trans-pore voltage increases the current signal, but it also increases translocation speed, so that small sequence-specific features $\sim$1 pA can not be resolved.

In this thesis, I will present a new approach to solve these issues by integrating the nanopore detectors with nanochannel devices in a micro/nanofluidic system.

Details include device concepts, fabrication process and theoretical analysis will be introduced in chapter 3.

1.4 Micro/Nanofluidics

Microfluidics is the study of fluidic systems in the 1-100 μm range. The development of micro/nanofluidic systems has significantly influenced various of subject areas from chemical synthesis and biological analysis to optics and even information technology [10]. For example, microfluidics can be used to study the growth of microbial populations [11], as well as for single cell separation [12] and developing inexpensive diagnostic device [13].

The fluidic behavior at the micro/nanoscale is different from 'macrofluidics' in a number of ways. For example, instead of gravity the factors that dominate the micro/nanofluidic system are surface tension, energy dissipation and fluidic resistance. In the macrofluidic system, turbulence flow that involves high momentum convection, low momentum diffusion is often observed, however flow in the micro/nanofluidic system are usually laminar flow that is characterized by high momentum diffusion and low momentum convection. The laminar flow normally exists in small dimensional and low Reynolds number (introduced in chapter 3.3.1) fluidic system. The electrokinetics of microfluidic systems, including electrophoresis and electroosmosis, are determined by the electric double layer (EDL) that forms at device surfaces in contact with an electrolyte solution(e.g. biological buffer). The first layer is the surface charge of the system due to the surface charged groups(e.g. silanol -OH for surfaces with silica chemistry). The second layer, known as the "diffuse layer", is composed of ions attracted to the surface via coulomb force. The characteristic thickness of the electric double layer is the Debye length, describing the screening (potential drops to e^{-1}) of electric fields

by surrounding charge carriers in the conductive environment. The typical Debye length of micro/nanofluidic system is in the order of nanometres, which is much smaller than the dimension of microfluidic system, however comparable to the lengthscale of nanofluidic system.

The technology of fabricating these micro/nanofluidic systems is called micro/nanofabrication that is originally developed for the integrated circuit industry. Typical techniques such as substrate growth, film deposition, resist patterning, etching and bonding, are involved in the fabrication process. Techniques that are utilized to make the nanopore-nanochannel integrated device will be introduced in details in chapter 3.

1.5 DNA in nanochannel confinement

In our experiment, the DNA molecule is confined in a nanoscale channel, thus understanding DNA dynamics and DNA conformation (e.g. DNA extension) in a confinement environment is important. The DNA molecule is considered to be self-avoiding chain, indicating that the chain occupies a finite volume and the segments can not overlap with each other. The effect of self-exclusion can be modelled using Flory theory. Consider a DNA chain, consists of interacting links of size a (a=2P, P is the persistence length, which describes the stiffness of a semi-flexible chain), with the effective width of w. In the Flory model, the exclusive volume of each link is $v_0 \sim a^2 w$. Consider the segments distributed in a volume $V \sim R_N^3$ (R_N is extent radius). The probability of a given segment will not overlap with another segment is:

$$P = 1 - v_0/V \tag{1.1}$$

For a chain consisting N segments, the probability that no distinct pairs will overlap is:

$$P^{\text{no}}_{\text{overlap}} = (1 - v_0/v)^{\frac{N(N-1)}{2}} = exp(\frac{N(N-1)}{2} ln(1 - v_0/v)) \approx \exp(-\frac{v_0 N^2}{2V}) \quad (1.2)$$

Given that probability of obtaining a polymer distribution with a given R_N for an ideal chain (no correlations, e.g. no self-avoidance) has a Gaussian distribution function:

$$P_{\text{ideal}}(N, R_N) = (\frac{3}{2\pi N a^2})^{\frac{3}{2}} \exp(\frac{3R_N^2}{2Na^2}) \quad (1.3)$$

Thus, the probability of a given chain conformation (extended radius R_N), with excluded volume interactions is the product of $P_{\text{ideal}}(N, R_N) \times P^{\text{no}}_{\text{overlap}}(N, R_N)$:

$$P = P_{\text{ideal}}(N, R_N) P^{\text{no}}_{\text{overlap}}(N, R_N) \approx \exp(-\frac{3R_N^2}{2Na^2} - \frac{v_0 N^2}{2R_N^3}) \quad (1.4)$$

Thus, the Flory free energy is:

$$\frac{F}{k_B T} = \frac{3R_N^2}{2Na^2} + \frac{v_0 N^2}{2R_N^3} \quad (1.5)$$

Minimizing the free energy, we get the equilibrium configuration (R_N) for a certain polymer chain:

$$\frac{\partial F}{\partial R_N} = 0 \quad (1.6)$$

Gives,

$$\frac{3R_N}{Na^2} - \frac{3v_0 N^2}{2R_N^4} = 0 \quad (1.7)$$

In a confinement free environment, the bulk volume of a DNA chain is $V \sim R_N^3$, thus,

$$R_N \approx a^{2/5} v_0^{1/5} N^{3/5} \approx (Pw)^{1/5} L^{3/5} \quad (1.8)$$

In a nanochannel confinement (channel dimension D), the bulk volume is $V \sim D^2 R_N$, thus,

$$R_N \approx a^{2/5} v_0^{1/5} N^{3/5} \approx \frac{(Pw)^{1/3} L}{D^{2/3}} \tag{1.9}$$

Besides the Flory model, there are some alternative theoretical models describing the behavior of DNA moelcules in nanochannel confinement according to the relative size of the channel dimension D and DNA persistence length P. For $D \gg P$, the environment confinement will have weaker effect on the DNA statistics. In this regime, the DNA chain can loop in the channel and the conformation will follow a self-avoiding random walk. However, when the channel dimension decreases and becomes comparable or even under the persistence length, bending energy starts to affect the chain statistics, coiling will significantly decrease and ultimately disappear, as shown in figure 1-3 A-C. Eventually, as looping is prohibited, chain contour can be only stored in successive deflections away from the channel surface, leading to a second type of behavior for the confined chain conformation. For $P^2/w \leqslant D \leqslant (Pw)^{1/5} L^{3/5}$, Pierre-Gilles de Gennes developed a theory to understand DNA statistics in the "blob" regime (figure 1-3 A). Considering the DNA chain in the nanochannel consists of self-avoiding blobs. The diameter of each blob is R_b, the DNA contour length is l_b. According to equation 1.8, the conformation (R_b) of etch blob can be expressed as $(Pw)^{1/5} L_b^{3/5}$, which is exactly the channel dimension D.

$$D = (Pw)^{1/5} L_b^{3/5} \tag{1.10}$$

Solve this equation, we have:

$$L_b = \frac{D^{5/3}}{(Pw)^{1/3}} \tag{1.11}$$

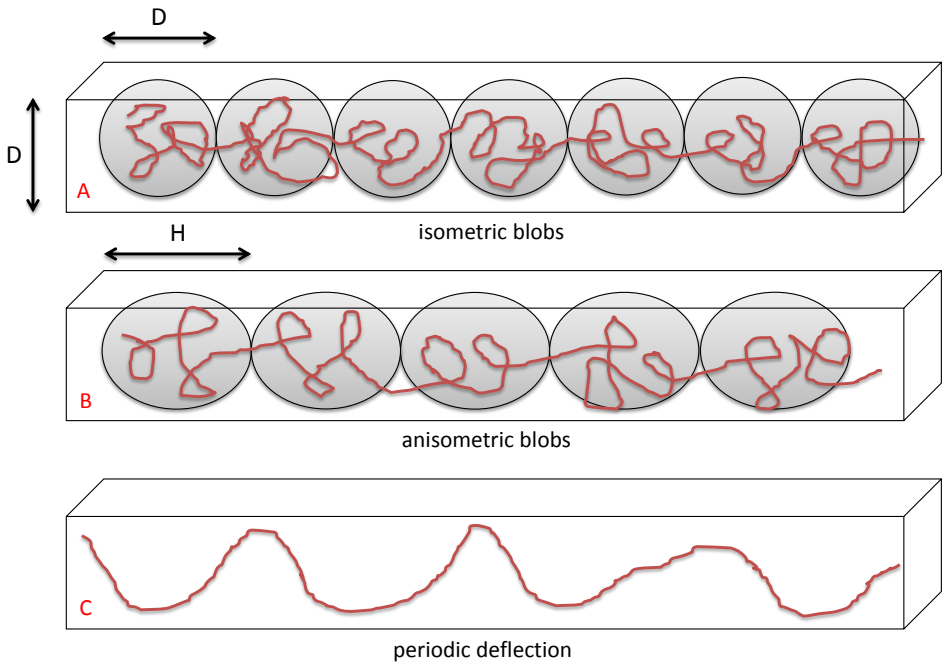

Figure 1–3: Different regimes of nanochannel confinement. A) de Gennes regime, B) extended de Gennes regime, C) Odijk regime.

Thus the extension of the DNA chain in this regime is simply the number of blobs ($\frac{L}{L_b}$) times the extension of each blob (D):

$$R_{\text{de Gennes}} = \frac{L}{L_b} D \tag{1.12}$$

Noting that L_b is given by equation 1.11, thus,

$$R_{\text{de Gennes}} = L \frac{(Pw)^{1/3}}{D^{2/3}} \tag{1.13}$$

The free energy of the chain is the number of blobs times $k_B T$:

$$F_{\text{de Gennes}} = k_B T \frac{L}{L_b} = k_B T \frac{(Pw)^{1/3}}{D^{5/3}} L \tag{1.14}$$

However as the channel dimensions decreasing, de Gennes models breaks down. For $2P \leqslant D \leqslant P^2/w$, Theo Odijk recently argued that a new regime exists where the symmetric blobs become anisometric (figure 1-3 B) as the DNA molecules being stretched out. The regime is called the "extended de Gennes regime". Assuming the anisometric blob has a width D perpendicular to the channel direction and an extended length H along the channel. Free energy of this system is given by the renormalized Flory free energy (equation 1.5) [14]:

$$F_{\text{Flory}} = \frac{R^2}{(L/L_b)H^2} k_B T + H \frac{(L/L_b)^2}{R} k_B T \tag{1.15}$$

Minimizing the Flory free energy gives $R = H(L/L_b)$ and $F_{\text{Flory}} = k_B T(L/L_b)$.

When the channel dimension D is below the persistence P, the bending energy significantly increases and dominates the hebavior of DNA. No coiling happens, the DNA chain undergoes periodic deflections with wall over the 'Odijk' scale $\lambda \sim (PD^2)^{1/3}$ [15].

The extension of DNA is the number of Odijk segments times the average length of each segment along the chain, given by $\lambda\cos(\theta)$, with θ the angle between segment and chain axis.

$$R_{\text{Odijk}} = L\cos(\theta) = L(1 - A(\frac{D}{P}^{2/3})) \tag{1.16}$$

A is a geometry-dependent numerical constant determined via simulation.

The total free energy is determined by k_BT multiple by the total number of Odijk segments in the polymer, L/λ:

$$F_{\text{Odijk}} = Bk_BT\frac{L}{\lambda} = Bk_BT\frac{L}{P^{1/3}D^{2/3}} \tag{1.17}$$

B is also a geometry-dependent scaling factor.

CHAPTER 2
Single-Molecule Detection Using Solid-State Nanopores

2.1 Experimental Setup

2.1.1 Silicon Nitride Membrane Window

Solid state nanopores are typically fabricated on insulating layers, silicon nitride (SiN_x) and silicon dioxide (SiO_2) thin membrane, by chemical etching or ion beam sculpting. In our experiment we fabricate nanopores on commercial silicon nitride membrane for TEM windows (bought from Silson and Norcada). The silicon nitride membranes,typically 10-50 nm thick, are suspended on the 200 μm thick silicon grid, which together constitute a 250×250 μm (50×50 μm for Norcada sample) window structure. To make these small windows, low stress silicon nitride membrane are deposited on 200 μm silicon wafer by low pressure chemical vapor deposition (LPCVD), followed by photolithography and silicon anisotropic etching.

2.1.2 Fluidic Cell

We are accessing the nanopore chip via a custom designed fluidic cell, shown in figure 2-2, which is made of polymethyl methacrylate (PMMA). The cell has two parts: a loading chuck and a sealing chuck. Three fluidic channels are drilled in each chuck for buffer exchange, one extra channel is drilled on both parts for anchoring Ag/AgCl electrodes. O-rings are fitted in the slot located at the center of both parts, nanopore chips are mounted in the loading chuck first and then sandwiched by the o-ring against the sealing chuck. After mounting the nanopore

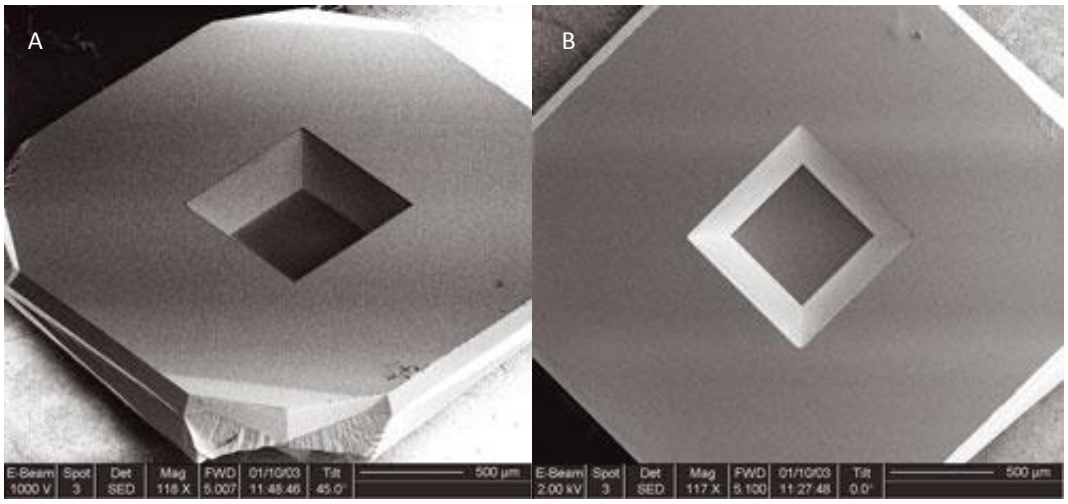

Figure 2–1: SEM image of silicon nitride membrane window for TEM. (Images from Silson Ltd.)

chip, the whole cell is tightened with screws and bolts to prevent electrolyte leakage (avoiding short circuit circumstances during measurements).

2.1.3 Faraday Cage

Minimizing electrical noise is crucial for performing high precision electrical measurements. Hence, the fluidic cell is mounted inside a custom designed Faraday cage for shielding electromagnetic fields. The Faraday cage consists of an inner and outer cage. Fluidic cell is placed inside the inner cage, which has special outlets drilled on the wall for electrodes. An ultra high precision headstage is mounted inside the outer Faraday cage.

2.1.4 DNA and buffer preparation

Lambda DNA, extracted and purified from lambda phage infected Escherichia *coli*, is used for our nanopore DNA translocation experiment. The λ-DNA molecule is a double-stranded DNA that has $\sim$ 48kbps, with 12-base single-stranded overhanging segments at both $5'$ ends. The two "sticky ends" join together and circularize the DNA molecule or form long concatemers. We purchased Lambda DNA

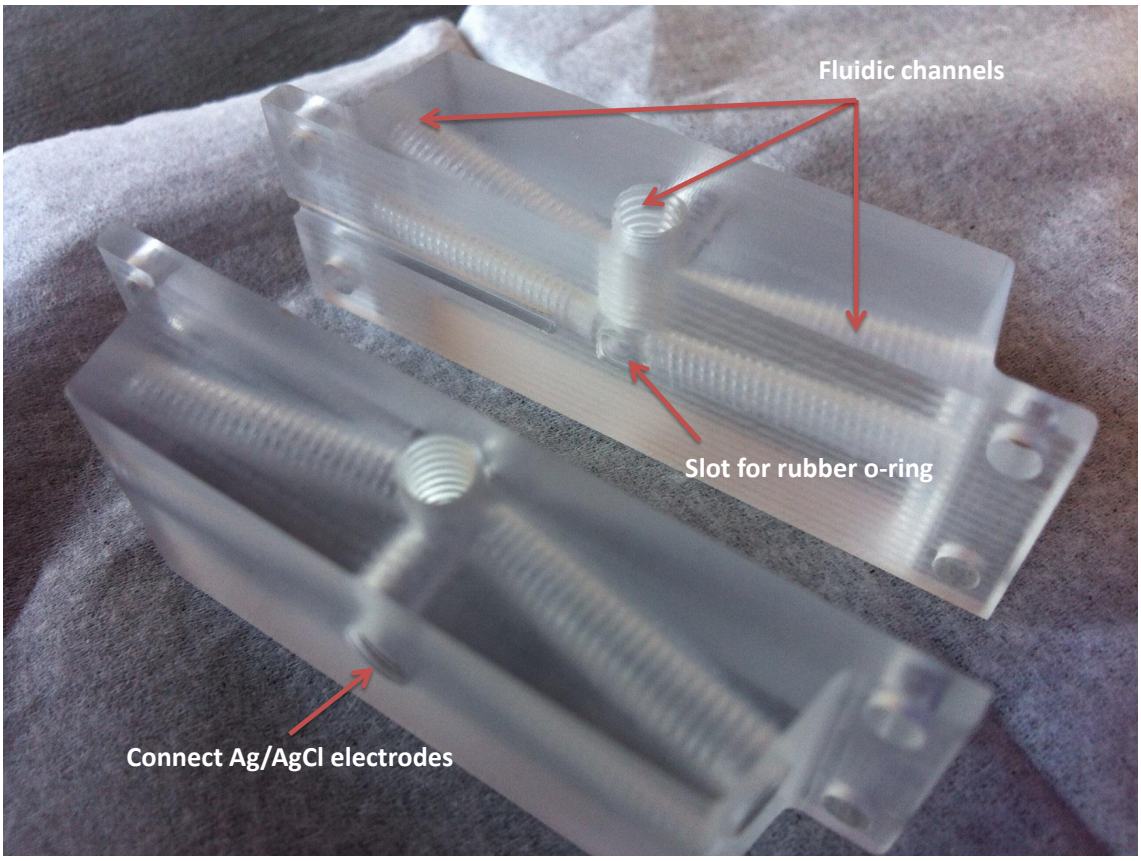

Figure 2–2: Disassembled view of PMMA fluidic cell. Three fluidic channels are drilled in each part, one extra channel are drilled for electrode.

(N^6-methyladenine-free),which is pre-dialyzed against 10 mM Tris-HCL (PH 8.0 at 20℃) and 1 mM EDTA, from New England Biolabs Inc for our experiment. In our experiment, lambda DNA with an original concentration of 500 μg/ml is diluted 50 times with TE(tris EDTA) buffer. Before mixing, the TE buffer (PH=8.0 at 20℃)is filtered with a 200nm Nylon filter and then degassed in a desiccator for at least 10 minutes. The goal of the filtering and degassing process is to remove dust particles as well as air bubbles that could potentially block the nanopore during experiment.

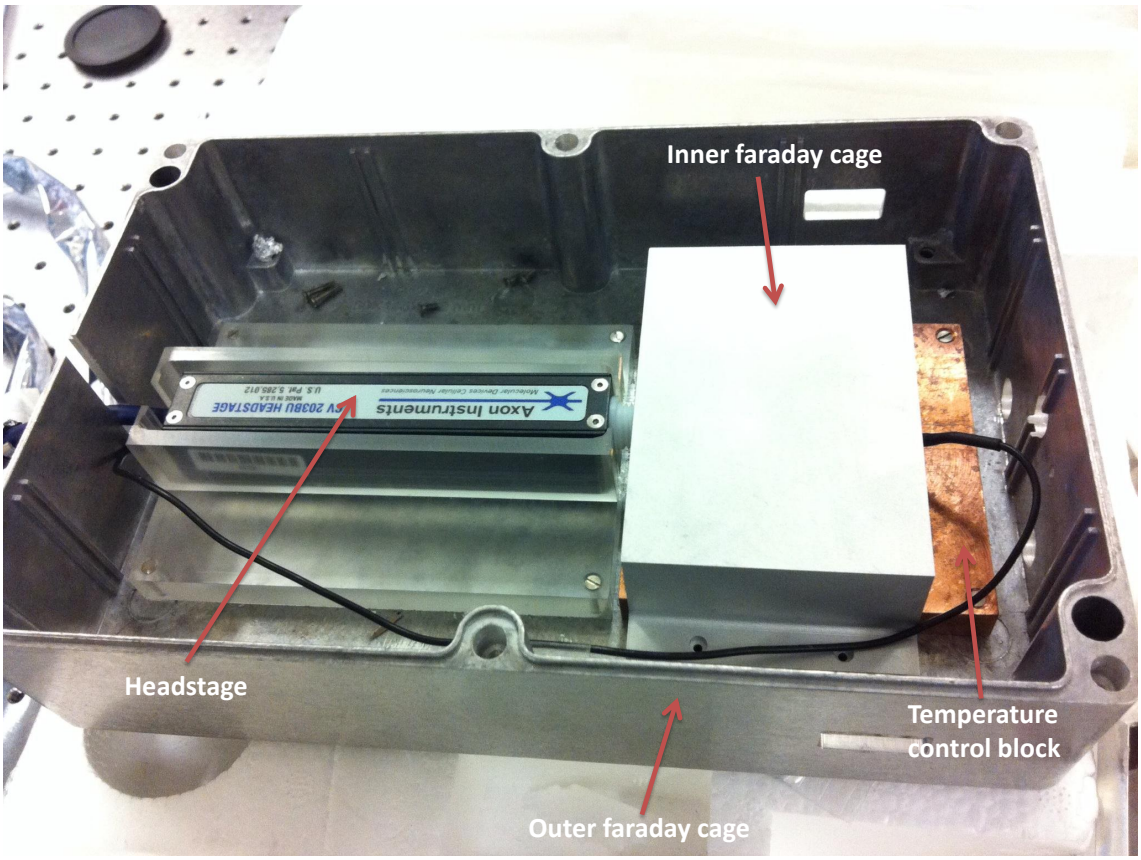

Figure 2–3: Experimental setup for nanopore experiment. Fluidic cell is placed in a inner Faraday and then the outer cage. Headstage is also placed inside the Faraday cage for the minimization of electric noise.

2.1.5 Measurement Apparatus

Hardware:

In order to measure the electrical signal of DNA molecules translocating through a nanopore configuration, picoampere (pA) sensitivity is required. We bought the Axopatch 200B (Axon Instruments, Molecular Devices), an ultra low noise patch clamp microelectrode amplifier that can achieve open circuit noise readings of $\sim$ 0.1pA rms at 10kHz bandwidth. For data acquisition, we also bought a specially designed self-contained highspeed data acquisition system – Digidata 1440A (Molecular Devices). The device has 16 analog input channels

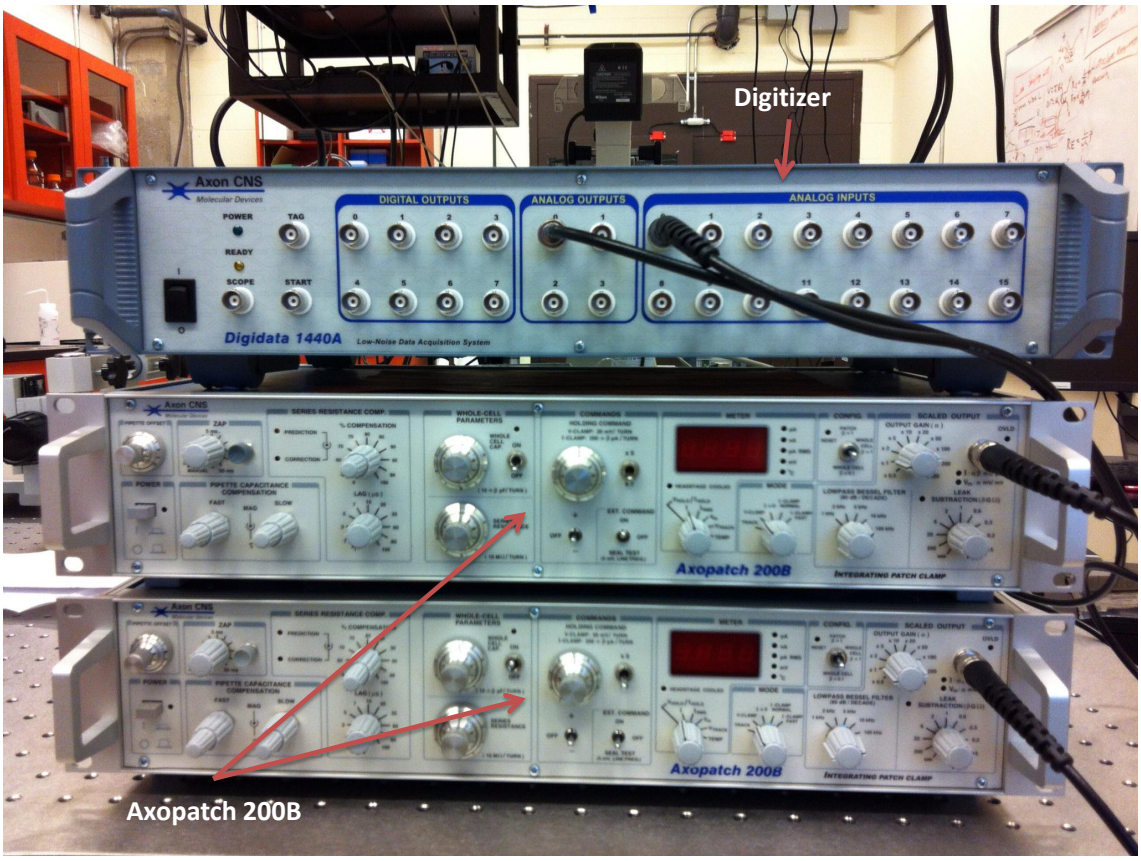

Figure 2–4: Figures of Axopatch 200B and Digidata 1440A (Molecular Devices) assembled on an optical table. Axopatch 200B is connected with fluidic cell and Digidata 1440A, Digidata 1440A is then connected with PC via USB cable.

and four analog outputs. Sampling rates range from 1-250 kHz. The system is rack-mountable can be easily connected to a PC via a USB interface.

Software:

For data analysis, p-camp software (Molecular Devices) is installed in a PC and then interfaced to a Digidata 1440A digitizer via USB cable. This is a comprehensive software package, designed specifically for use with the Digitdata 1440A, for controlling data acquisition and analyzing signal channel current recordings with a minimum of programming. The p-clamp software in particular is optimized for visualizing and analyzing long single channel recordings, important in

nanopore experiments where there is a need to quickly navigate recordings that can be on order of 1-24 hours in length. We also developed a custom MATLAB program (by David Laleyan) to analyze recorded data. The codes generated from the raw data plot the blocking current(ΔI) versus dwell time(τ) (figure 2-5) histograms, enabling different type of current blockades to be detected and distinguished.

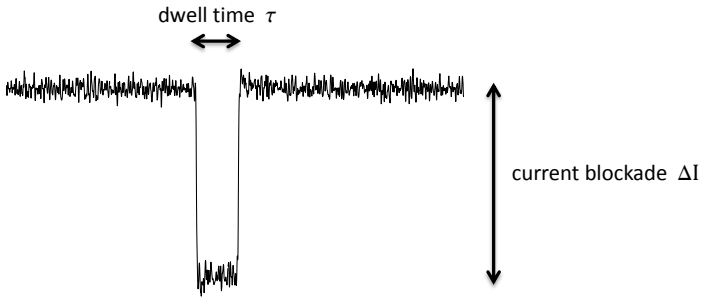

Figure 2–5: Enlarged view of a typical blockade signal associated with a DNA molecule translocating through a nanopore. Dwell time (τ) is the time DNA molecules stay inside the nanopore, blocking current (Δ I) is the trans-current drop when the DNA molecules pass through a nanopore.

2.2 Experimental Protocol

2.2.1 TEM Nanopore drilling

In 2001 Jiali Li et al developed a method for creating nanoscale pores in an insulating solid-state membrane. They called their technique "ion beam sculpting" [8]. To create a nanopore, they first fabricated a large ($\sim$0.1 mum diameter) bow-shaped cavity on silicon nitride membrane. Ar^+ ions are accelerated and then sputtered on the membrane, subsequently drilled a nanopore with a typical diameter of $\sim$ 60nm. Finally, the nanopore is then ion-sculpted using 3-keV Ar^+

ions. After being exposed in the accelerated Ar^+ ions, instead of increasing size, the nanopore pore on the silicon nitride membrane shrunk to ∼1.8 nm, indicated by the transmitted ion counting rate.

Two years later, A. J. Storm from Cees Dekker's group, developed a second technique for nanopore fabrication: "electron beam ablation" [9]. Nanopores, with the size of ∼ 1-20 nm, are first fabricated on thin amorphous membrane (e.g. silicon dioxide or silicon nitride), by electron-beam lithography followed by anisotropic etching or direct drilled with TEM by finely focusing the electron beam on membrane. Once the pore was formed, it was either larger (typically for nanopores fabricated via EBL + Anisotropic etching) or smaller (typically for nanopores drilled via TEM) than the desired diameter. To achieve a desired size nanopore, the nanopore was then exposed under high energy electron beam in a TEM. Due to the fluidizing of surrounding material and driving forces caused by surface tension, we can both shrink the nanopore by exposing it under expended electron beam or enlarge it via focusing the beam on the nanopore edge. Once the desired diameter is achieved, electron beam will be switched off, material quenches and retains its shape. Single-nanometre precision can be achieved with this technique.

For our experiment, we drilled nanopores directly on free standing silicon nitride membrane by finely focus electron beam (beam diameter $\leqslant$ 4 nm)on the membrane via TEM. After focusing the electron beam on membrane for a few minutes (5 to 10 min), a pore with the initial diameter of ∼4 nm was formed. Since the desired pore diameter for our experiment is around 10 nm, electron beam was then focused on the edge of the nanopore, removing material rapidly, subsequently expanding the nanopore to a desired diameter. Experiments were

carried out in a 200 kV field emission TEM from JEOL, model JEL-2100F at Polytechnique Montral's Center for Characterization and Microscopy of Materials (the $(CM)^2$). The current density was $1 \times 10^8 \mathrm{A} \cdot \mathrm{m}^{-2}$, and the electron beam was focused over a 4 nm spot in diameter at a magnification of ×500 or ×600k for drilling. Nanopores were imaged in the same TEM, at a magnification of ×250k or ×300k. A fluence of 10^5 $e{\cdot}\mathrm{nm}^{-2}$ or lower was used for imaging nanopores, an order of magnitude lower than fluences used for shrinking a nanopore by electron beam illumination, so that the pore would remain stable during imaging. Figure 2-6 shows four nanopores in different sizes fabricated with the JEL-2100F.

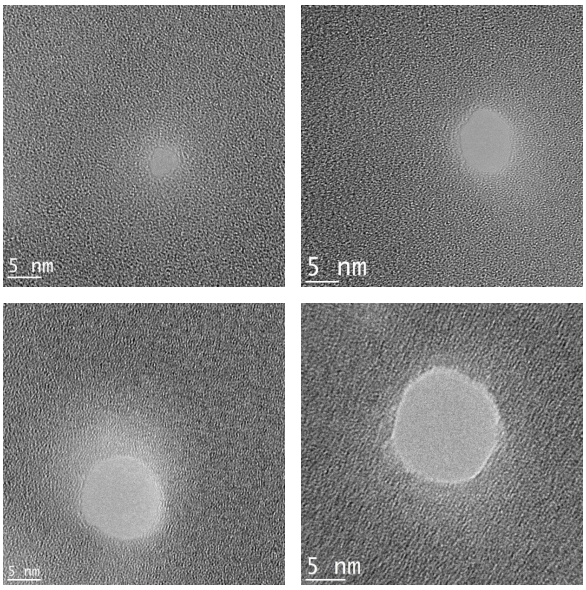

Figure 2–6: Nanopores in different sizes: A)3.7 nm pore, B) 6.8 nm pore, C)11.9 nm pore, D) 13.5 nm pore. All nanopores are fabricated by TEM on 30nm thick silicon nitride membranes. Experiments were carried out at Characterization and Microscopy of Materials, the $(CM)^2$ located in Ecole Polytechnique de Montreal. TEM model JEL-2100F from JEOL.

2.2.2 Nanopore cleaning

After fabrication nanopores are cleaned with Piranha solution or Nanostrip. Piranha is a mixture of sulfuric acid (H_2SO_4) and hydrogen peroxide (H_2O_2) (typical ratio 3 : 1) frequently used in microelectronics industry to remove organic residues(e.g. photoresist) off substrates. Piranha solution is a strong oxidizer and effective hydroxylation reagent(adding OH groups). After cleaning process, residues on the substrate will be completely removed and the substrate surface will become extremely hydrophilic. Outside of the cleanroom, we use a chemical called Nanostrip, which is basically a stabilized verison of Pirhana (less reactive, lower chance for gas-generation during storage and consequently lower risk of explosions) Nanostrip is a mixture of sulfuric acid, peroxymonosulfuric acid, hydrogen peroxide and water. We tried both piranha and nanostrip cleaning for our experiment. There is no clear difference regarding the results. We make the Piranha solution by adding 10ml hydrogen peroxide(30% H_2O_2 from J.T. Baker) into 30ml sulfuric acid(98% from J.T. Baker). The solution is then heated to 90℃on a hotplate. Nanopores are dipped in the Piranha solution for at least 30 minutes. Afterwards, pores are rinsed gently with degassed DI water. The nanostrip protocol is the same as the piranha protocol (except for the mixing step).

2.2.3 Nanopore Mounting and Characterization

To make a good seal as well as avoiding unwanted blockages(nano-bubbles and dust particles), the nanopore chip is blow-dried with a nitrogen gun and then sealed in the fluidic cell via rubber o-rings. All aqueous solution(KCl solution DI water and isopropanol) are degassed in a sonicator for 10 minutes and pumped in a desiccator for 10 minutes to remove air bubbles. In order to avoid dust

particles, solutions are pre-filtered by a 200 nm Nylon filter. The fluidic cell is wetted with isopropanol, then DI water, and finally 1M KCl solution. Afterwards, two Ag-AgCl electrodes are dipped inside the KCl solution, and then the whole cell is placed inside the inner Faraday cage. Once the nanopore is electrically characterized (for example: I-V curve, PSD, current trace) and verified to be functional, we run the nanopore DNA translocation experiment. Diluted lambda DNA molecules are pipetted very close to the pore region, a voltage potential $\sim$ 100mV is applied across the two electrodes, finally we record and analyse DNA translocation data.

2.3 Results and Discussion

2.3.1 Nanopore Electrical Characterization

The first step is to perform an IV curve measurement for electrical characterization of the nanopore. Figure 2-7 shows an example of I-V measurement in 1M KCl solution for two different nanopores. In these experiments, a linear I-V curve was observed. Linear fits to the data yield the value of the nanopore resistance. We observe that as the nanopore diameter decreased from 15.6 to 7.9 nm, the resistance increased from 12.98 to 35.49 MΩ.(Figure 2-7)

2.3.2 Noise Reduction

To reduce the dielectric noise, we coat a thin polydiemthylsiloxane(PDMS) layer(around 10 μm) on the silicon nitride surface surrounding the nanopore area (figure 2-8), this technique was reported by Vincent Tabard-Cossa [16]. A significant difference of the PSD at 100mV was observed, between samples with and without PDMS coating. After coating with PDMS layer, PSD drops by 10$\sim$100 times in the low frequency region, shown in figure 2-9, indicating that it improves the dielectric properties of the support chip.

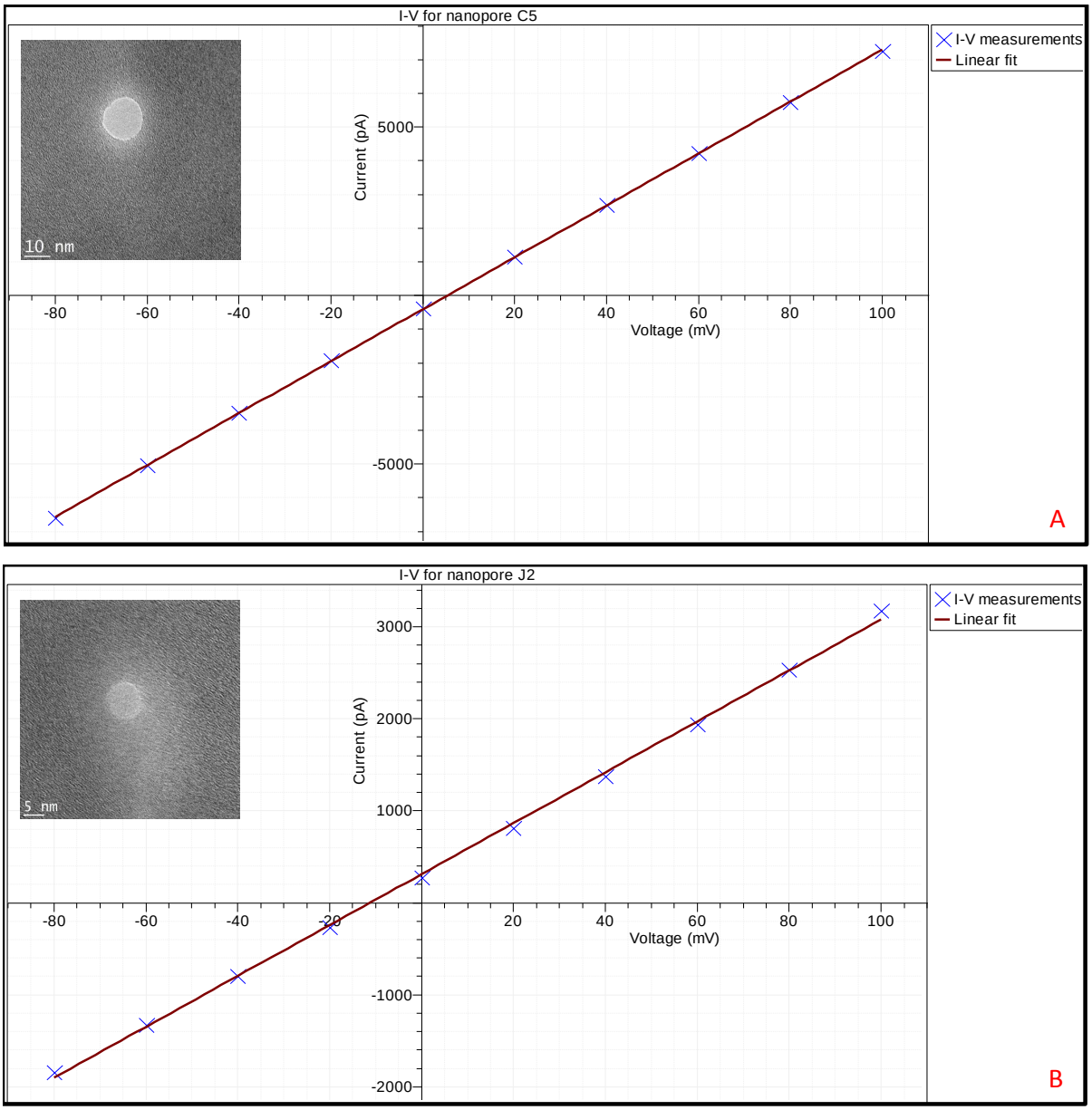

Figure 2–7: I-V measurements and linear fits for two different nanopores. A) pore size 15.6 nm, conductance 77.041±0.003 nS,fitting correlation coefficient 0.995141, B) pore size 7.9 nm, conductance 28.179±0.003 nS, fitting correlation coefficient 0.972062.

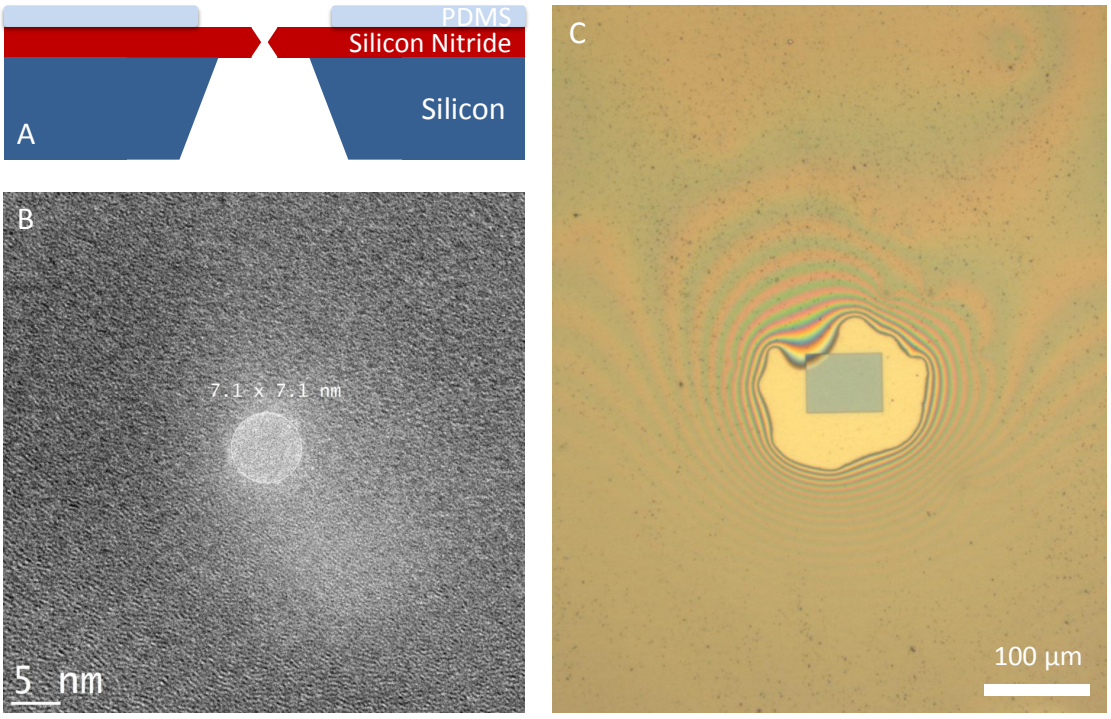

Figure 2–8: PDMS Coating.A) Cross-sectional view of the nanopore chip, illustrating where the PDMS is coated. B) TEM image of nanopore been coated. C) Optical microscope image of the PDMS-coated nanopore support chip (top view), grey rectangle showing in the centre is the free-standing silicon nitride membrane.

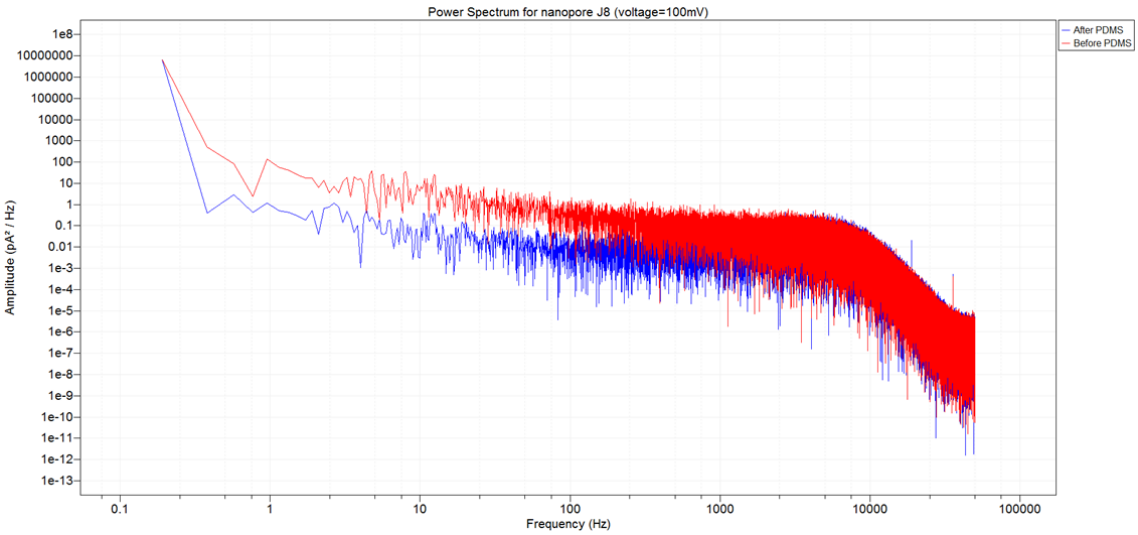

Figure 2–9: Power spectrum density of the same nanopore chip before(red line) and after(blue line) PDMS coating.

2.3.3 Lambda DNA Translocation

A voltage of 150 mV was applied across the nanopore, with buffer solution (1 M KCl, 10 mM Tris, 1 mM EDTA, pH 8.0, 2 ml each side) in the seperated cell chambers. Cations (K^+) and aions (Cl^-) are driven through the pore configuration by a strong electric field(10^6V/m). The ion flow produces a stable base current(around several nanoamperes, shown in figure 2-10 A). Subsequently, 20 μl of 50 mg/ml lambda-DNA solution diluted in KCl was pipetted close to the pore region. After a few minutes, DNA diffuses towards the pore region the pore region and is then pulled by the electric field through the nanopore. Consequently, transient current dips (blockades) along the current trace are observed (figure 2-10 B). The width of each current blockade along the time axis represents the dwell time of molecule acrossing the pore region. As observed, dwell time varies from 100 μs to 1 ms (figure 2-10 C).

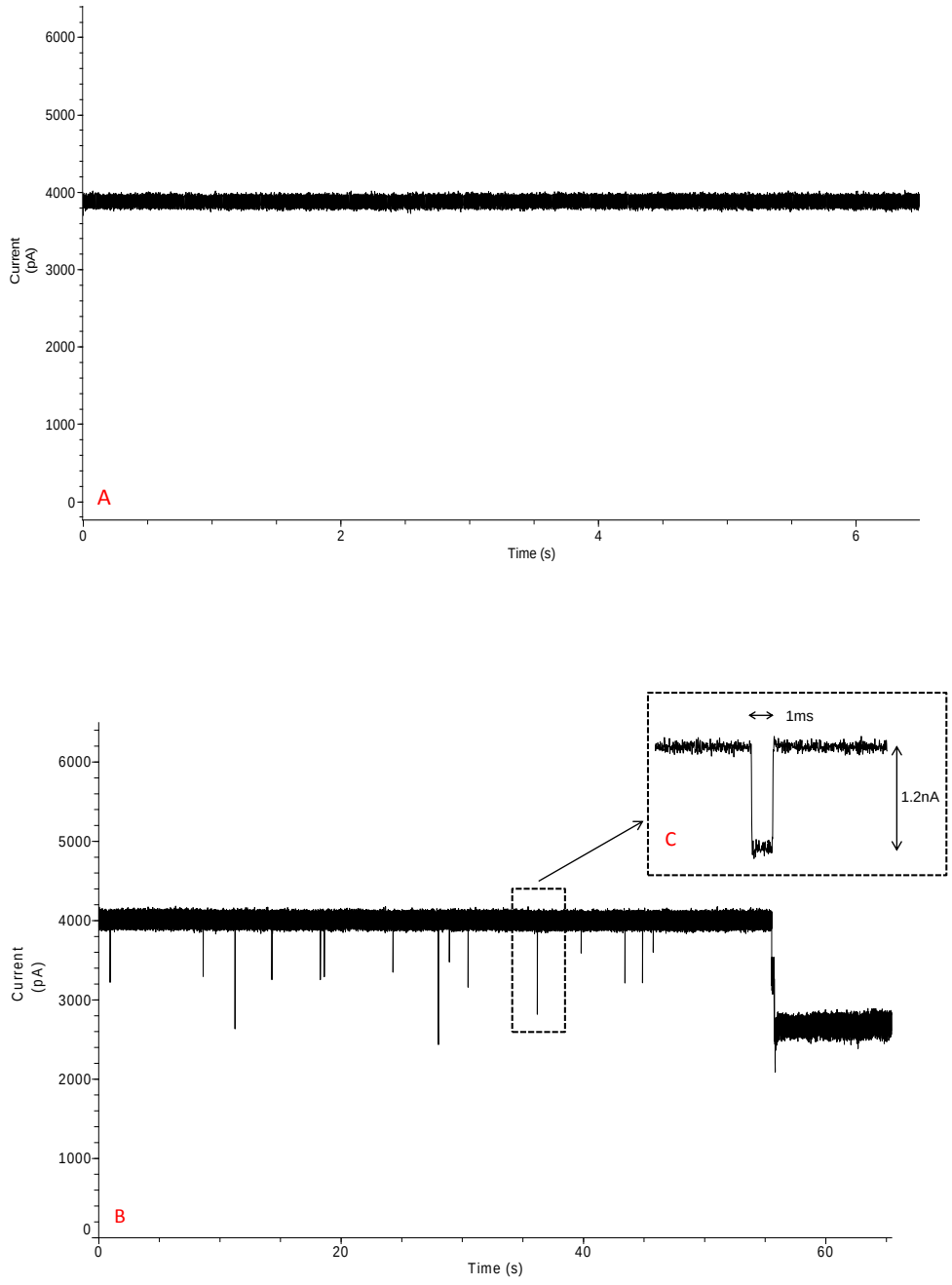

Figure 2–10: Current trace before and after adding Lambda-DNA. A) before adding Lambda-DNA, current is stable with no blockades. B) After adding Lambda-DNA, current trace with blockades was observed.

2.3.4 DNA Conformation Analysis

In 2003, Jiali Li from Golovchenko's group reported [17] the discovery of multi-level structure in DNA translocation blockades. While translocating through a nanopore, DNA molecules block the ionic flow and cause a drop in the current trace. If the molecules are folded during translocation, multi-level blockade structure will be observed (see figure 2-11). The expected current blockade from a dsDNA molecule translocating through a nanopore will depend on the geometry of the pore, the electrolyte composition as well as DNA associated counterions [16], [18]. However, we can still explain our data by simplifying the theoretic model with a first-order approximation (assuming cylindrical pore and ignoring edge effects) [16], the relative current change is:

$$\Delta I / I_{open} = \Delta S_{DNA} / S_{pore} \tag{2.1}$$

and the current blockage is:

$$\Delta I = \sigma V \Delta S_{DNA} / S_{pore} \tag{2.2}$$

with ΔI the current blockage amplitude, I_{open} the open pore current, ΔS_{DNA} the DNA cross section area pore region, S_{pore} the nanopore cross section area, σ the solution conductivity, and V the applied voltage.

The equation above gives a linear relationship between the ΔS_{DNA}(DNA cross section area) and ΔI(current blockages), which means the amplitude of current blockage is proportional to the DNA cross section area determined by the amount of DNA in the nanopore at one time. For the current signal shown in figure 2-10 B, the amplitude of single level current blockage is $\sim 0.4\,\mathrm{nA}$ the open pore current is $4.1\,\mathrm{nA}$, the pore diameter is $8.1\,\mathrm{nm}$. Solving equation 2.1 for ΔS_{DNA},

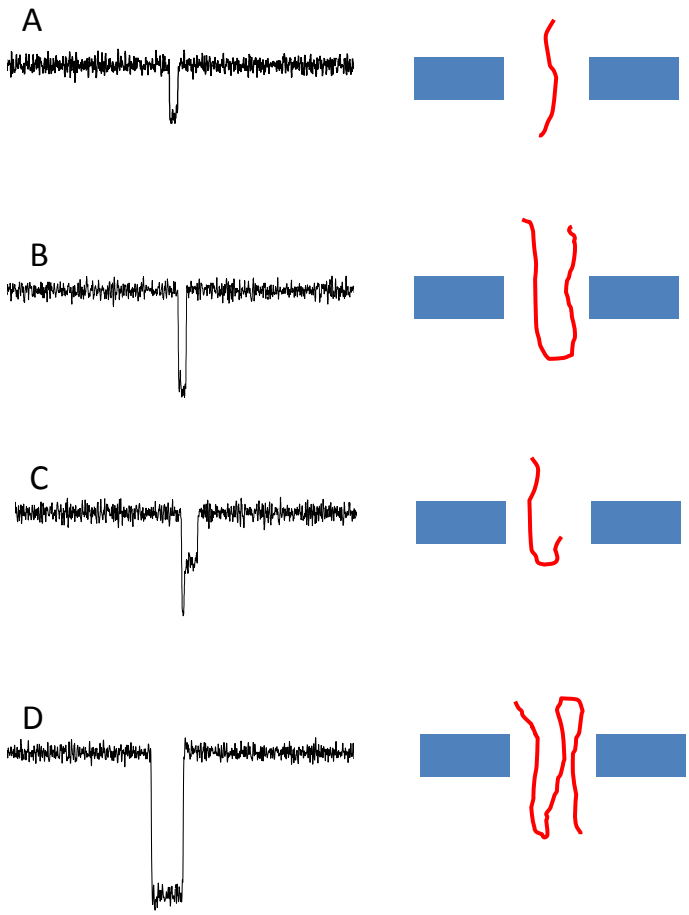

Figure 2–11: Different types of translocation signals, indicating different conformation of the DNA molecule: A) single DNA no folding, B) double folded near the end, C) double folded, D) triple folded.

we obtained an reasonable value for the hydrodynamic diameter of dsDNA of $\sim$ 2.5 nm. As shown in figure 2-11, different types of blockade are observed referring to different DNA conformation.

CHAPTER 3
Single-Molecule DNA Analysis and Manipulation Using Nanopore-Nanochannel Device

3.1 Introduction

Nanopore and nanochannel based devices are robust methods for biomolecular sensing and single DNA manipulation. Nanopore-based DNA sensing has attractive features that make it a leading candidate as a single-molecule DNA sequencing technology. Nanochannel based extension of DNA, combined with enzymatic or denaturation-based barcoding schemes, is already a powerful approach for genome analysis. There is revolutionary potential in devices that combine nanochannels with nanpore detectors. In particular, due to the fast translocation of a DNA molecule through a standard nanopore configuration, there is an unfavorable trade-off between signal and sequence resolution. With a combined nanochannel-nanopore device, based on embedding a nanopore inside a nanochannel, we can in principle gain independent control over both DNA translocation speed and sensing signal, solving the key draw-back of the standard nanopore configuration.

In this chapter, I will introduce the device concept, perform theoretic analysis of the fluidic system as well as present fabrication process and preliminary results we have.

3.2 Device Concept

The nanopore-nanochannel fluidic device consists of a nanochannel embedded with a nanopore. The nanochannel runs between two loading microchannels,

microchannels are connected to different reservoirs that serve as the entrance of buffer. This chip is then sealed with a 0.15 mm glass cover slide via low temperature bonding. To better access the device, we bond the sealed nanopore-nanochannel chip to a PDMS layer. The PDMS layer, which has millimetre scale channels on one side, is pre bonded to a 75×50×1 mm(2.95 × 1.96 × 0.040") glass slide. The whole chip is then sealed in a specially designed fluidic cell,via o-rings and a top aluminium retaining ring. The fluidic cell is designed to be able to provide fluidic, pressure, electric and optical access. Device layout is shown in figure 3-1.

DNA molecules are driven inside a nanochannel by pressure. Due to the one dimensional confinement, dsDNA molecules will be stretched alone the nano-scale channel, laying across the nanopore detector. When a voltage is applied across the pore region, negatively charged DNA molecule will be locally captured to the pore region by electric field.(figure 3-2) Given that DNA molecular width is around 2.5 nm, and DNA persistence length P is around 50 nm in the salt condition (2 × TBE) we used, theoretically, we can fabricate a pore around or below the molecular width, and apply a voltage that is small enough will only attract the DNA to pore region instead of pushing it through. Ionic flow (K^+, Cl^-) across the pore region will be blocked by the DNA molecule that lies across it, thus produces a blockade containing DNA structural information in the current trace. Importantly, this device is designed to have independent control over translocation speed and sensing signal. We can independently control the tanslocation speed by finely tuning pressure difference(ΔP), therefore we can scan any target region on a DNA chain as long as we need. Subsequently, a stable blockade signal

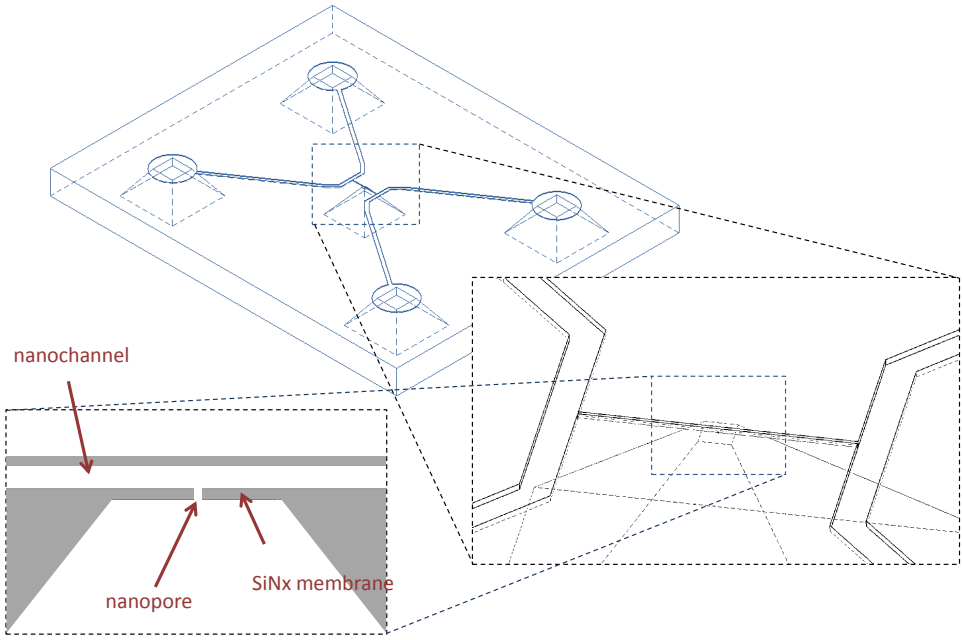

Figure 3–1: The geometry of nanopore-nanochannel device. A) geometry of the whole nanopore-nanochannel chip including channels and reservoirs, B) nanochannel are connected by 2 loading microchannels, C) cross-section of the nanopore-nanochannel structure.

could sustain longer enough for the nanopore detector to sense the structural information of any target region.

The DNA molecule is pushed along the nanochannel by pressure applied across different reservoirs (typically 300 mbar), translocation speed can be controlled manually by adjusting pressure. A open pore current could be obtained if there is no DNA in the nanochannel. This open pore current is considered to be the base current for electrical sensing.

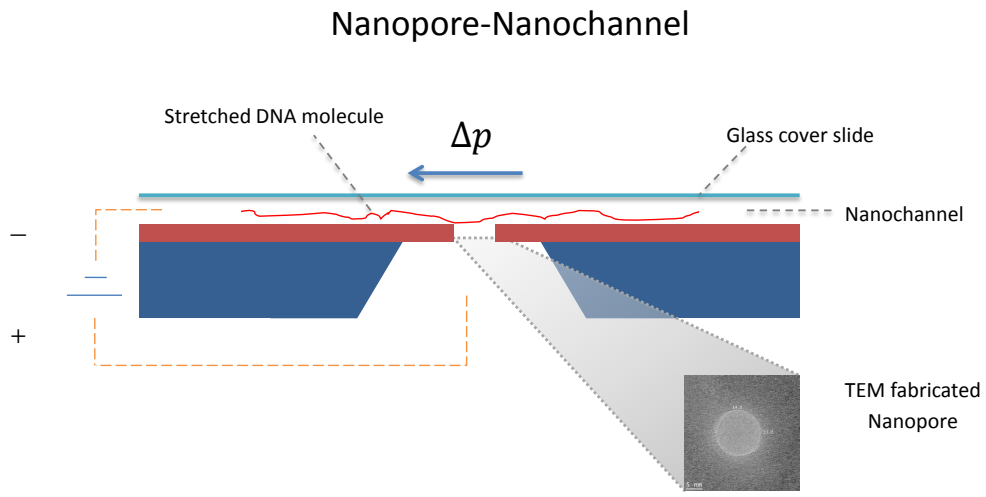

Figure 3–2: The concept of nanopore-nanochannel device. One DNA molecule is pushed inside the nanochannel by pressure, DNA are stretched by the channel and lies across the nanopore detector.

This novel nanopore-nanochannel integrated fluidic device could significantly push the limit of nanopore sensing to single-nanometre scale with a commonly used silicon nitride nanopore. Further more, there are two approaches to increase the device resolution:

1) Fabricate smaller nanopore. Nanopores that have smaller diameter(around or smaller than dsDNA molecular width, 2.5 nm) could sense structural information of a smaller region along the chain, so that fewer base pairs ($\sim$ 7 bps for a 1 nm pore) will contribute to the final blockade signal.

2) Fabricate narrower nanochannel. Nanochannel with a smaller dimension(around or below dsDNA persistence length, 50 nm) will provide stronger confinement for

dsDNA molecule. DNA will be stretched to a longer conformation along the channel [19]. Scanning along a pre-stretched DNA molecule, nanopore detector could provide us structural information containing fewer base pairs.

3.3 Theoretical Analysis

3.3.1 Hydraulic resistance and Reynolds number

In order to understand the flow behavior inside a micro/nano-fluidic system, as well as for better control over DNA translocation speed in our device, we need to introduce the concept of hydraulic resistance. For a certain fluidic channel size and configuration, a constant pressure drop Δp results in a certain constant flow rate Q. This result could be written as the Hagen-Poiseuille law:

$$\Delta p = R_{hyd} Q = \frac{1}{G_{hyd}} Q, \tag{3.1}$$

The proportionality factors R_{hyd} and G_{hyd} in equation 3.1 is defined as the hydraulic resistance and conductance, respectively. Eq 3.1 is the hrdrodynamic analog to Ohm's law, $\Delta V = RI$ (ΔV is the electric potential drop, R is the electric resistance, I is the current).

Ohm's law	Hagen-Poiseuille law
$\Delta V = RI$	$\Delta p = R_{hyd} Q$
$[\Delta V]$ V	$[\Delta p]$ Pa
[I] A	[Q] $\frac{m^3}{s}$
[R] Ω	$[R_{hyd}]$ $\frac{Pa \cdot s}{m^3}$

Table 3–1: Ohm's law and Hagen-Poiseuille law

The table above compares Ohm's law and Hagen-Poiseuille law, as well as SI units. Remarkably, for low Reynolds number systems, the rules of circuit theory can be applied to the equivalent hydrodnamic channel array, replacing electrical

resistances with hydraulic resistances. Thus calculating the parallel coupling of two channels with hydraulic resistance R_1 and R_2, the law for parallel electric resistance, $\frac{1}{R} = \frac{1}{R_1} + \frac{1}{R_2}$, can be used. The effective hydraulic resistance of two paralleled channels is given by:

$$R_{hyd} = \frac{R_1 R_2}{R_1 + R_2} \tag{3.2}$$

Consistently, the effective hydraulic resistance of two channels in series is given by:

$$R_{hyd} = R_1 + R_2 \tag{3.3}$$

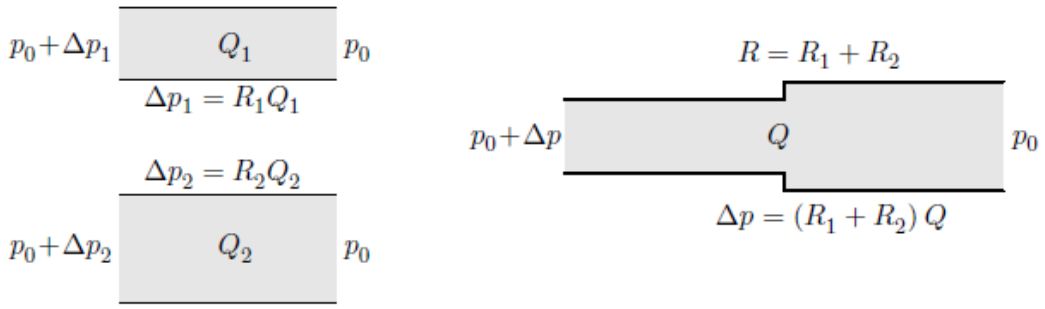

Figure 3–3: The series coupling of two channels with hydraulic resistance R_1 and R_2. The simple additive law R = R_1+R_2 is only valid in the limit of low Reynolds number, Re $\to$ 0, and for long narrow channels. [20]

However, equation 3.2 and 3.3 given above, are only valid in the limit of low Reynolds number ($Re \leq 1$) and for long narrow channel. In fluid mechanics, the Reynolds number (Re) is a dimensionless number that gives a measure of the ratio of inertial forces to viscous forces and consequently quantifies the relative

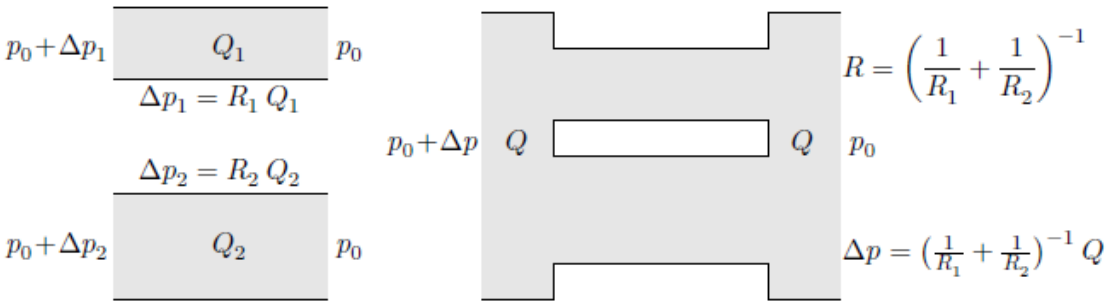

Figure 3–4: The parallel coupling of two channels with hydraulic resistance R_1 and R_2. The additive law for the inverse resistances $R^{-1} = R_1^{-1} + R_2^{-1}$ is only valid in the limit of low Reynolds number, Re $\to 0$, and for long narrow channels far apart. [20]

importance of these two types of forces for given flow conditions. It's determined by the following equation:

$$Re = \frac{\rho v L}{\mu} = \frac{v L}{\nu} \tag{3.4}$$

v is the mean velocity of the object relative to the fluid, L is the characteristic linear dimension, μ is the dynamic viscosity of the fluid, ν is the kinematic viscosity, ρ is the density of the fluid. In our case, L is around $200\,nm$ (given by the length of the nanochannel), v is around 1×10^{-6} m $\cdot\, s^{-1}$, ρ is 1.0×10^3 kg $\cdot\, m^{-3}$, μ is 1.0×10^{-3} Pa $\cdot$ s (we take the dynamic viscosity μ and density ρ of water at 20 for simplification).

Thus Re is given by:

$$Re = \frac{\rho v L}{\mu} = \frac{1.0 \times 10^3 kg \cdot m^{-3} \times 10 \times 10^{-6} m \cdot s^{-1} \times 200 \times 10^{-6} m}{1.0 \times 10^{-3} Pa \cdot s} = 2{\times}10^{-3} \ll 1 \tag{3.5}$$

Since the Reynolds number of our nanopore-nanochannel device is far smaller

than 1, equation 3.2 and 3.3 are applicable for our case. We can calculate the hydraulic resistance R_{hyd} of a given shape channel by solving the Navier-Stokes equation with assigned boundary conditions for the Poiseuille flow. For a circle shape straight channel with radius a, channel length L, the hydraulic resistance R_{hyd} is:

$$\frac{8}{\pi}\eta L\frac{1}{a^4} \tag{3.6}$$

The hydraulic resistance for a rectangle shape channel with height h, channel width w, length L is:

$$\frac{12\eta L}{1-0.63(h/w)}\frac{1}{h^3 w} \tag{3.7}$$

For the nanopore-nanochannel device, a 20 nm nanopore is drilled at the center of the nanochannel, the dimension of the nanochannel is 160 nm $\times$ 200 nm $\times$ 200 μm(160 nm in depth, 200 nm in width, 200 μm in length). The nanopore is a cylinder shape with diameter equals to 20nm, length equals to 40nm. Figure 3-5 shows an equivalent circuit for the nanopore-nanochannel connection. Electrolytic solution is driven inside the nanochannel from one end, and then pushed out from the other end as well as the nanopore. Now we can compare the flux of both exits by calculating their hydraulic resistance. According to figure 3-5, $R_{halfchannel}$ and $R_{nanopore}$ are in parallel, thus the ratio of electrolytic flux flowing through the nanopore is given by $\eta = \frac{R_{halfchannel}}{R_{halfchannel}+R_{nanopore}}$, $R_{halfchannel}$ is the hydraulic resistance of half the nanochannel (nanochannel are separated into 2 parts, because the nanopore is drilled in the center position of the channel), $R_{nanopore}$ is the hydraulic resistance of nanopore. $R_{nanopore}$ and $R_{halfchannel}$ is given by equation 3.6 and 3.7.

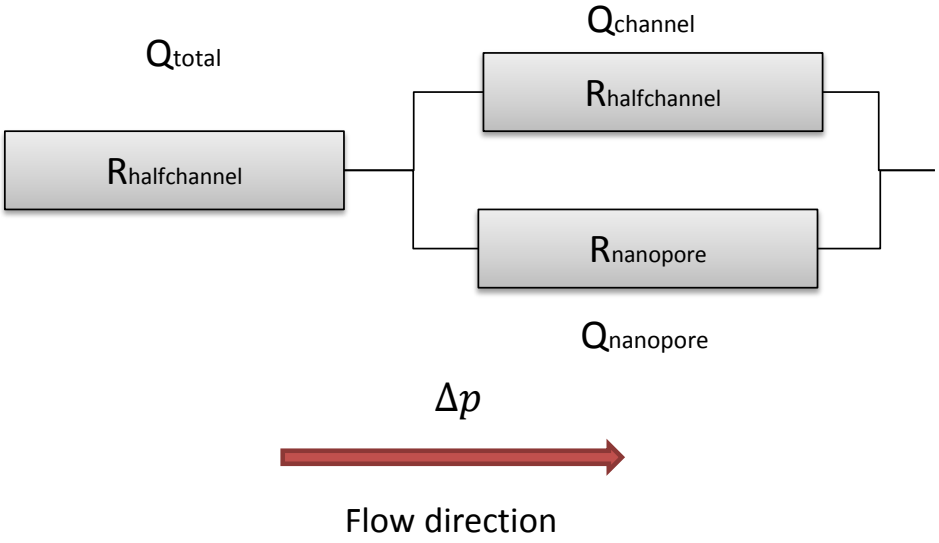

Figure 3–5: Equivalent circuit for the nanopore-nanochannel connection. A pressure Δp is applied across the nanochannel and nanopore. Electrolytic solution flowing through half of the nanochannel, and then split into two flows, one continued its path (flux $Q_{channel}$), one turned 90 degree flowing through the nanopore (flux $Q_{nanopore}$).

Thus η is given by:

$$\eta = \frac{R_{halfchannel}}{R_{halfchannel} + R_{nanopore}} \tag{3.8}$$

$$= \frac{\frac{12\eta L_{halfchannel}}{1-0.63(h/w)}\frac{1}{h^3 w}}{\frac{12\eta L_{halfchannel}}{1-0.63(h/w)}\frac{1}{h^3 w} + \frac{8}{\pi}\eta L_{nanopore}\frac{1}{a^4}} \tag{3.9}$$

$L_{halfchannel}$ is 100 μm, h is 140 nm, w is 200 nm, $L_{nanopore}$ is 40 nm, a is 10 nm. Thus according to equation 3.8, η equals to 0.225, which means only 22.5 % of the fluid will go through the nanopore. However if the size of nanopore shrink by half, namely 5 nm, this ratio significantly drops to 1.4%. As the pore diameter

becomes smaller and smaller, the hydraulic resistance of the pore can be made 100 x higher than the nanochannel, so only a very small amount of fluid will be forced through the pore by the applied pressure.

3.3.2 Scaling argument

In the previous subsection, we hypothesize that once the nanopore diameter is small enough, DNA molecule will lay across the nanopore instead of translocating through the pore. We will prove this result via a simple scaling argument and in addition determine the critical diameter below which DNA molecule will not enter the pore spontaneously.

We first consider the situation without electrical field, shown in figure 3-6. The probability (p) of a DNA molecule going into the nanopore configuration is determined by three energy terms: the energy acale associated with thermal fluctuations $E_{thermal}$, the free energy difference between the nanochannel confinement polymer and the polymer in bulk ΔF and the bending energy $E_{bending}$ required to pull the polymer through the pore. Firstly, the thermal energy is on the order of k_BT.

Secondly, the free energy difference of DNA molecule is determined by the energy barrier between one-dimensional confinement state in the nanochannel and the confinement free state in the bottom reservoir. If we consider the DNA molecule as an ideal chain, this energy difference is given by

$$\Delta F = \frac{Pl}{D^2} k_B T, \tag{3.10}$$

with P the persistence length of the DNA molecule, l the length of DNA molecule in the pore region, and D is the channel dimension.

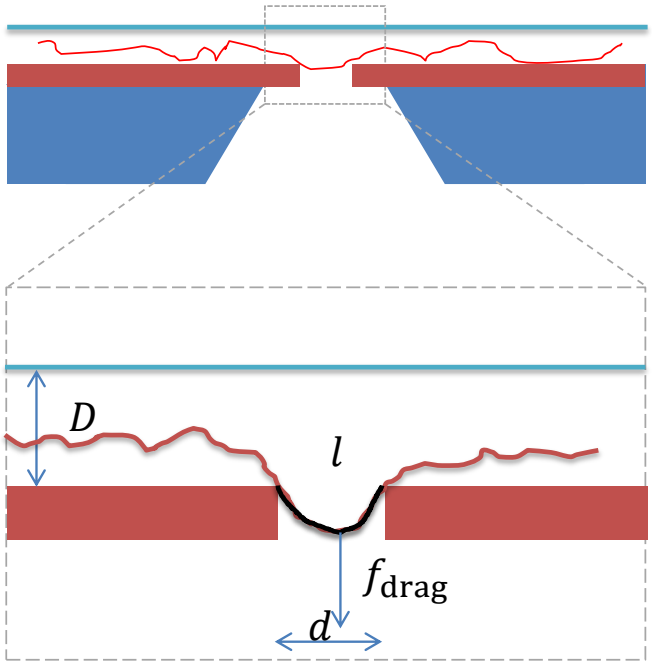

Figure 3–6: A cartoon of dsDNA molecule entering the nanopore. The DNA molecule is stretched across the pore, and a segment of length l(drawn as black line in the figure) of the DNA molecule has entered the pore area. The quantity D is the channel dimension, d is the pore diameter, l is the segment length, and f_{drag} is the drag force caused by free energy difference.

Finally, DNA molecules have to overcome the bending energy in order to go through the nanopore. Consider DNA as a chain of Kuhn segments connected to its nearest neighbors by a torsion spring (spring constant K), then we can calculate the amount of energy required to bend it into a coil of radius R. The relationship between stiffness (persistence P) and spring constant K is

$$K = Pk_BT \tag{3.11}$$

Like a linear spring where the energy is of the form

$$E = \frac{1}{2}Kx^2 \tag{3.12}$$

The energy to bend the chain is of the form

$$E = \frac{1}{2}Kl(\frac{dt}{ds})^2 \tag{3.13}$$

where $\frac{dt}{ds}$ is the derivative of the tangent vector to each Kuhn segment of the chain. Since the chain is being bent into a circle of radius R, $\frac{dt}{ds} = \frac{1}{R}$. Thus the bending energy is

$$E_{bend} = \frac{1}{2}\frac{Kl}{R^2} = \frac{1}{2}\frac{Pl}{R^2}k_BT \sim \frac{Pl}{R^2}k_BT \tag{3.14}$$

As shown in figure 3-6, the channel dimension D is around 200 nm, the length l is around half a circle with radius d, $l \sim \frac{\pi d}{2} \sim d$, d is the pore diameter around 20 nm, R is the pore radius around 10 nm, P is the persistence length of DNA molecule that is around 50 nm (these data are taken from our real experiment). As shown in equation 3.10, 3.11 and 3.15, the first two terms of energy, $E_{thermal}$ ΔF, has a certain probability $p \sim e^{-\frac{E}{k_BT}}$ to push the DNA molecule inside the pore, however the last term of energy $E_{bending}$ prevents the DNA molecule entering the pore region. Thus, once we equate the two parts of energy we know the critical diameter d.

$$E_{thermal} + \Delta F = E_{bending} \tag{3.15}$$

$$E_{thermal} \sim k_BT \gg \Delta F \sim \frac{Pl}{D^2}k_BT \tag{3.16}$$

According to equation 3.16, the thermal fluctuation energy is at least 10 times higher ($\frac{Pl}{d^2} \sim \frac{1}{40}$) than the free energy difference, which means $E_{thermal}$ is dominating among the energy that push DNA molecules inside pore region.
For simplification we equate $E_{thermal}$ to $E_{bending}$,

$$E_{thermal} \sim k_B T \sim E_{bending} \sim \frac{Pl}{R^2} k_B T \tag{3.17}$$

thus,

$$k_B T \sim \frac{Pl}{R^2} k_B T \tag{3.18}$$

which gives,

$$\frac{Pl}{R^2} = 1 \tag{3.19}$$

We already know $l \sim d$, thus,

$$d_{critical} \sim P \tag{3.20}$$

Interestingly, the critical diameter $d_{critical}$ is just in the order of persistence length P (50 nm). Which means, if we fabricate a nanopore with diameter under P, DNA molecule will be confined inside the nanochannel instead of going through the nanopore. However, if we increase the pore diameter, the probability p of DNA molecule translocating through the pore will increase significantly, DNA will go through the pore spontaneously without being pulled by any external force, electrical attraction for instance.

For nanopore-nanochannel device with nanopore diameter $\geq$ 50 nm, once DNA molecule entered the pore area, there will be a constant pulling force f_{drag} (shown in figure 3-6) caused by free energy difference ΔF,

$$f_{drag} = \frac{\partial \Delta F}{\partial l} \sim \frac{P}{D^2} k_B T \tag{3.21}$$

This constant drag force f_{drag} will pull the DNA molecule through the pore continuously.

3.4 Device fabrication

3.4.1 Introduction

A number of different fabrication strategies have been developed to create nanochannel and nanopore devices. Nanochannels are typically fabricated via conventional nanofabrication technology, an electron beam lithography (EBL) step followed by reactive ion etching (RIE). Next, photolithography (PL) followed by RIE can be used to make loading microchannels that will interface the device's nanofluidic dimensions with bulk fluidic reservoirs. Nanopores, as mentioned in Chapter 2, can be fabricated via a classic strategy developed by Dekker and coworkers at Deflt, involving direct milling of pores via a focused electron beam. Utilizing the same technique, using the JEOL TEM at Polytechnique's Center for Characterization and Microscopy of Materials (the $(CM)^2$), we are able to make nanopores with size varying from 1 to 100 nm.

Our objective is to fabricate a device that combines the advantages of nanopore-based DNA sensing and nanochannel based single molecular DNA analysis: electrical-based nanoscale interrogation with efficient DNA linearization. The fabrication process of the nanopore-nanochannel device is challenging as it involves integration of the classic nanopore and nanochannel fabrication methodology. A nanochannel is etched across a suspended thin silicon nitride membrane via EBL/RIE. The etch depth of nanochannel is tuned so that only 20-40 nm of material is left inside the channel. A nanopore is subsequently drilled inside the nanochannel in a TEM and micro-scale access channels are created to introduce

DNA-containing buffer. Lastly, it is necessary to bond the device to create enclosed fluidic channels, the most challenging part of the fabrication process. Figure 3-7 shows an over view of the fabrication process, the following sub-sections will be focused on details of each process as well as special fabrication strategies we used.

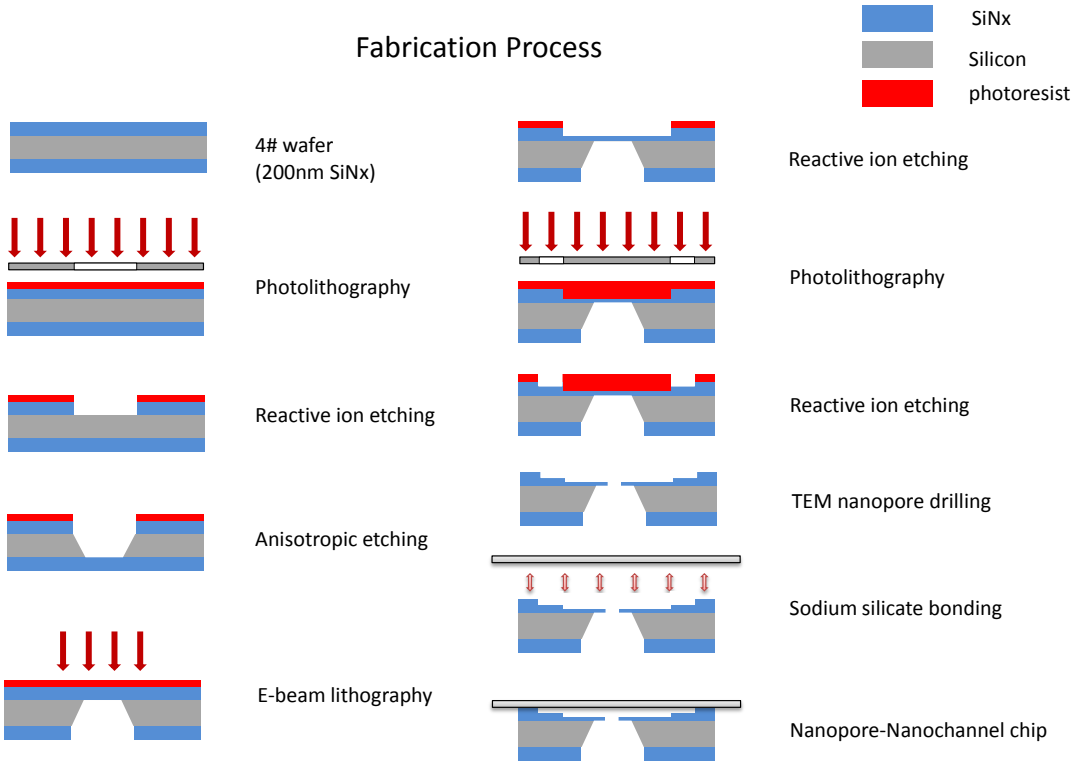

Figure 3–7: Overview diagram of the nanopore-nanochannel chip fabrication process.

3.4.2 Wafers

The fabrication of nanopore-nanochannel devices begins with 4 inch wafers bought from Cornell Nanofabrication Facility (CNF). The wafer is coated with silicon nitride thin film on both side. Figure 3-12 shows the cross-sectional schematic

of the wafer: 400 μm thick silicon is sandwiched by two layers of 200$\pm$10 nm thick silicon nitride material. For deposition of silicon nitride layers on substrates, two methods are applicable:

1. Low pressure chemical vapor deposition (LPCVD) technology, which works at rather high temperature (700-850°C) is usually accomplished in a vertical or in a horizontal tube furnace [21].

2. Plasma-enhanced chemical vapor deposition (PECVD) technology that works at relatively low temperature (below 400°C) and vacuum conditions [22].

The synthesis reaction for generating silicon nitride film by PECVD or LPCVD is different:

PECVD: 3 $SiH_4(g)$ + 4 $N_3(g)$ $\rightarrow$ $Si_3N_4(s)$ + 12 $H_2(g)$

LPCVD: 3 $SiCl_2H_2(g)$ + 4 $NH_3(g)$ $\rightarrow$ $Si_3N_4(s)$ + 6 $HCl(g)$ + 6 $H_2(g)$

Silicon nitride film from CNF are deposited on silicon substrate by plasama enhanced chemical vapor deposition (PECVD) via GSI Plasma Enhanced Chemical Vapor Deposition (PECVD) system. Deposition rate is 1100$\mathring{A}$/min, silicon nitride film refractive index is 2.0, tensile stress is 500 Mpa at 400°C, 207 Mpa at 250°C.

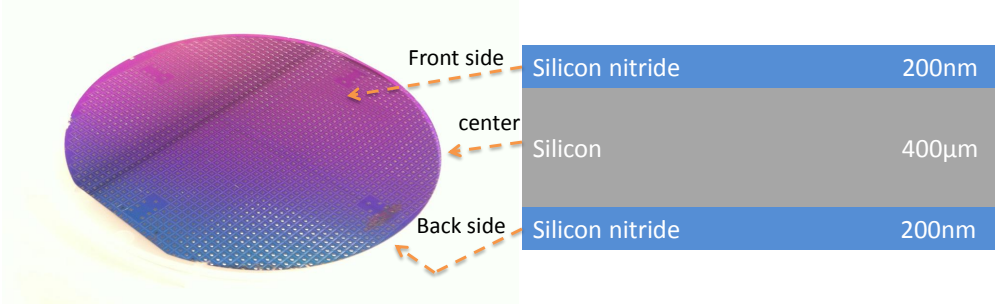

Figure 3–8: Cross sectional view of silicon nitride coated wafer used in our experiment.

3.4.3 Fluidic Reservoirs

Photolithography

Fluidic reserviors are fabricated on the wafer by a standard photolithography process followed by reactive ion etching and silicon anisotropic etching. To remove organic residuals on surface, wafer is first immersed in acetone for 30 s then rinsed with isopropanol and DI water. Silicon nitride surface is hydrophilic after the cleaning process reducing the adhesion of a thin positive-type photoresist to the silicon nitride surface. Lack of adhesion between silicon nitride surface and photoresist will cause photoresist blisters during UV exposure [23]. The blister defects will become a serious issue for complicated device fabrication. Applying hexamethyldisilazane (HMDS) to the SiN surface prior to coating photoresist will improve the resist adhesion by changing the Si_3N_4 surface property from hydrophilic to hydrophobic. All wafers are treated with HMDS for 30 s and spin-dried. Shipley 1813 positive photoresist, 1.4 μm thick, is coated on the wafer via an automatic spin coater.(Figure 3-9 B) Wafer is soft baked at 115°C for 60 s and then aligned with photomask in the contact aligner. Uncovered photoresist is then exposed at UV light with a total dosage of 90 mJ/cm^2.(Figure 3-9 C) The wafer is then developed in Microposit MF 319 developer for 45 s. As exposed resist is removed by developer, special windows are opened in the resist layer for RIE process. (Fig 3-9 D)

Reactive Ion Etching

Resist-patterned wafers are loaded in the MERIE P5000 system, etched with reactive ions to create open windows on silicon nitride film. The etching process begins with a 30 s stabilization with gas flow: CHF_3 30 scc, Ar 70 scc, CF_4 7 cc.

Afterwards, plasma is initiated by applying a strong RF (radio frequency) electromagnetic field. This step takes $\sim$ 120 s (etching speed around 1.7 nm/s, this may vary) to etch away 200 nm thick silicon nitride. CHF_3 and CF_4 flow is then turned off, residuals are evacuated in the Ar flow for 15 s. (Figure 3-9 E)

Silicon Anisotropic Etching

Anisotropic etching is the fact that some wet etchants etch crystalline materials at very different rates depending on different crystal faces. For single-crystal silicon, several anisotropic wet etchants are available: potassium hydroxide (KOH) has an etching rate selectivity of 400 $\times$ in <100>/<100> direction; EDP (ethylene diamine and pyrocatechol) has a <100>/<111> selectivity of 17 $\times$; Tetramethylammonium hydroxide (TMAH) presents a safer alternative than EDP, with a 37 $\times$ selectivity in <100>/<111> direction, however it etches silicon nitride at a higher rate than KOH [24]. In our process, we tried both TMAH and KOH, and found that KOH is much friendly to silicon nitride membrane, thus resulting a higher success rate for fabrication.

After the RIE process, uncovered silicon nitride is etched away leaving square openings on the membrane. Remaining membrane serves as a mask for silicon protecting it from been etched in the following step. Wafers are cleaned with Piranha and then dipped in TMAH (tetramethylammonium hydroxide) or KOH bath for $\sim$ 12 hours (etching speed 33.3 μm/hour, this may vary). Operation temperature of TMAH bath is setted to be 85 $\pm$2 °C. Wafers are profiled via Ambios XP200 Profiler every other hour to calculate etching speed and total etching time. Subsequently, silicon reservoirs of pyramid shape are created on the wafer with 200 nm thick silicon nitride membranes suspending on one side. (See Figure 3-10)

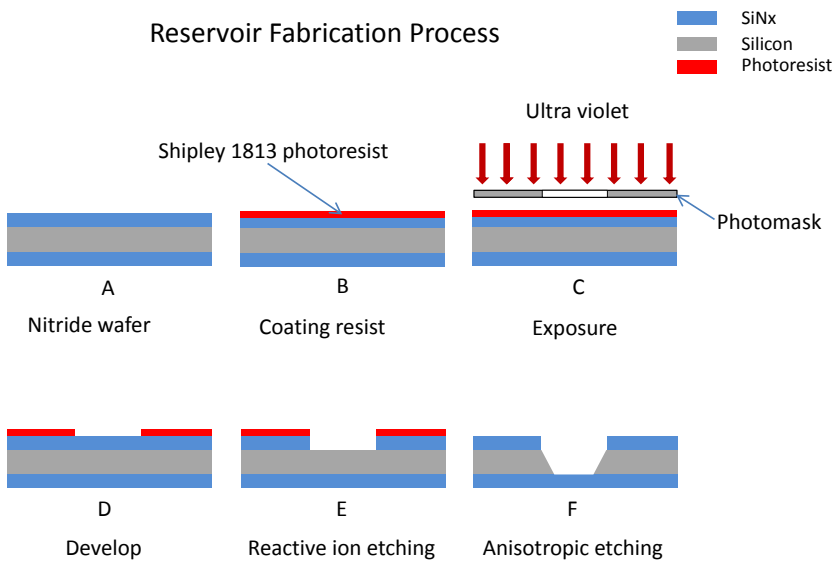

Figure 3–9: Cross sectional schematic of fluidic reservoir fabrication process.

3.4.4 Nanochannels

E-beam Lithography

Nanochannels are fabricated via electron beam lithography (EBL) step followed by reactive ion etching. In e-beam lithography a focused beam of electrons is scanned in a pre-determined pattern across a resist coated surface. The exposed resist is subsequently removed by a chemical developer. E-beam lithography has an ultra high resolution (10 nm or smaller) limited mainly by forward scattering of electrons with in the resist.

In our experiment, wafers are first cleaned by piranha solution (Figure 3-11 A). Then a layer of ZEP520A e-beam resist is coated on one side of the wafer which has suspended silicon nitride suspended membranes(Zep resist has excellent plasma resistance, compared with more conventional positive resists like

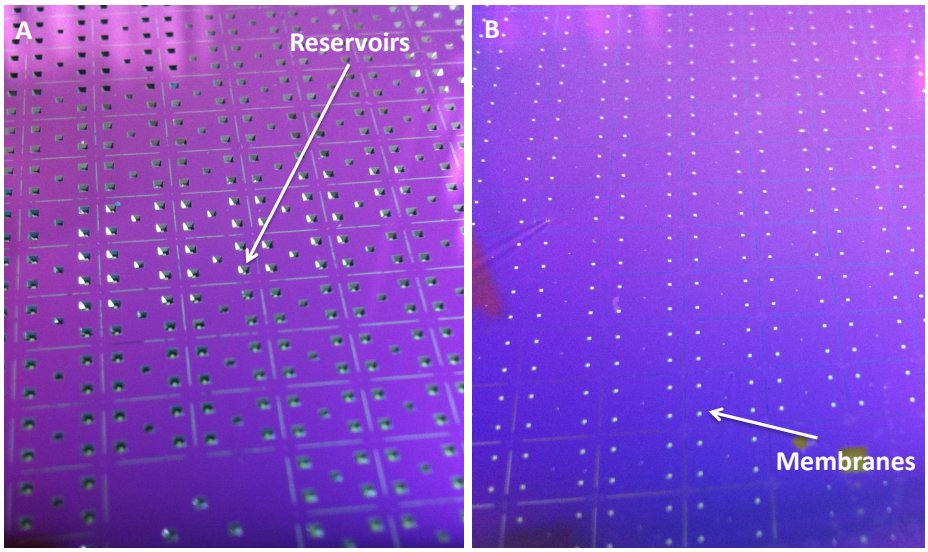

Figure 3–10: Anisotropic etched reservoirs on silicon nitride/silicon/silicon nitride wafer. A) 5 reservoirs are etched on etch sample, four on the corner , one in the center. B) suspended silicon nitride membrane on the other side of wafer, corner membrane $120 \times 120\,\mu m^2$, center membrane $75 \times 75\,\mu m^2$.

PMMA).(Figure 3-11 B) The wafer is then loaded in the VISTEC VB6 UHR-EWF(ultra-highresolution-extendedwidefield) e-beam system with a typical resolution of 25 nm. Afterwards, high tension is turned on, electron beam is directly writing on the ZEP resist following the desired nanochannel pattern(Figure 3-11 C). Since ZEP520A is a positive resist, the exposed regions is removed during the following developing process(Figure 3-11 D).

Reactive Ion Etching

In order to fabricate a 160 nm deep nanochannel across the 200 nm thick silicon nitride membrane without damaging or etching it through, slower etching speed and precisely calibration is required. We modified the RIE protocol, removing magnetic field during the main etching step, to meet this requirement.

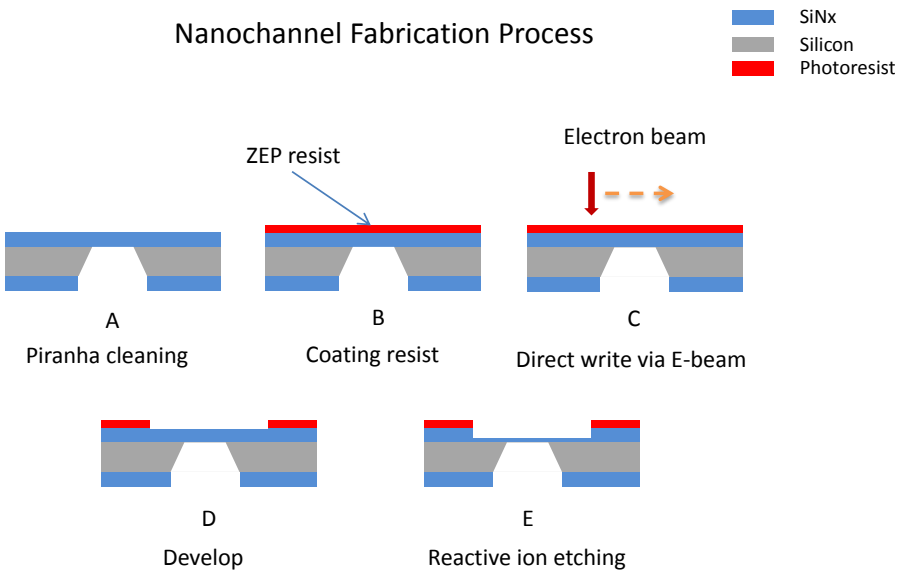

Figure 3–11: Nanochannel fabrication process.

This results in a lower etching speed $\sim 1.3\,\mathrm{nm/s}$ (original etching speed $1.7\,\mathrm{nm/s}$) for silicon nitride. Calibration experiments of various etching duration(30 s, 60 s, 90 s, 120 s and 150 s) at the same condition are done for precisely measuring etching speed. Wafers with nanochannel-patterned resist are then loaded in the RIE system. After been etched for around 100 s (this may vary depending upon the condition of instruments, e.g. temperature, gas flow), nanochannels with the dimension of 160 nm in depth, 200 nm in width, 200 μm in length are fabricated in the center of each sample.(Figure 3-11 E)

3.4.5 Loading Microchannels

Photolithography

Loading microchannels are designed for the interface of nanofluidic dimensions with fluidic reservoirs. To create these channels, the wafer is first cleaned

in piranha solution for 30 min. Given that sample wafers have fragile membrane structures, all wafers are spin-dried at 1000 rpm instead of being blow-dried with nitrogen gun. The Wafers are then treated with HMDS for 30 s and coated with 1.4 μm thick Shipley 1813 photoresist. After baking at 115 °C for 60 s, resist is patterned in the contact aligner with a total UV dosage of 90 mJ/cm^2 and then developed in MF319 for 45 s.

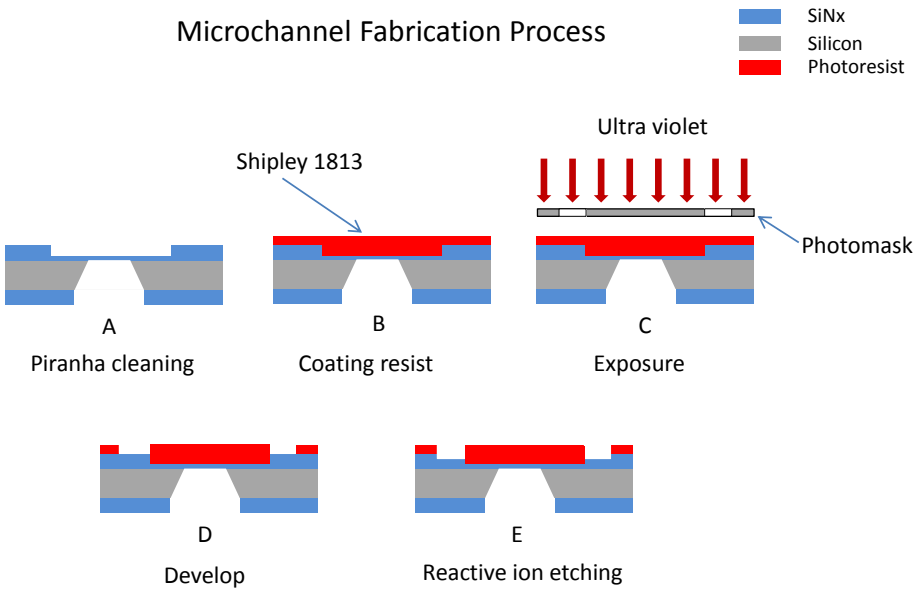

Figure 3–12: Diagrams of microchannel fabrication process.

3.4.6 Reactive Ion Etching

Subsequently, wafers are loaded in the RIE system and etched for around 90 s. Two U-shape microchannels which has the dimension of 50 μm in width, 120 nm in depth are created on the silicon nitride layer.(Figure 3-13 A) Each microchannel is connected with the nanochannel in the center, as well as connecting two fluidic

reservoirs (thin membranes located the four corner of each device are destroyed in order to connect microchannels with reservoirs).

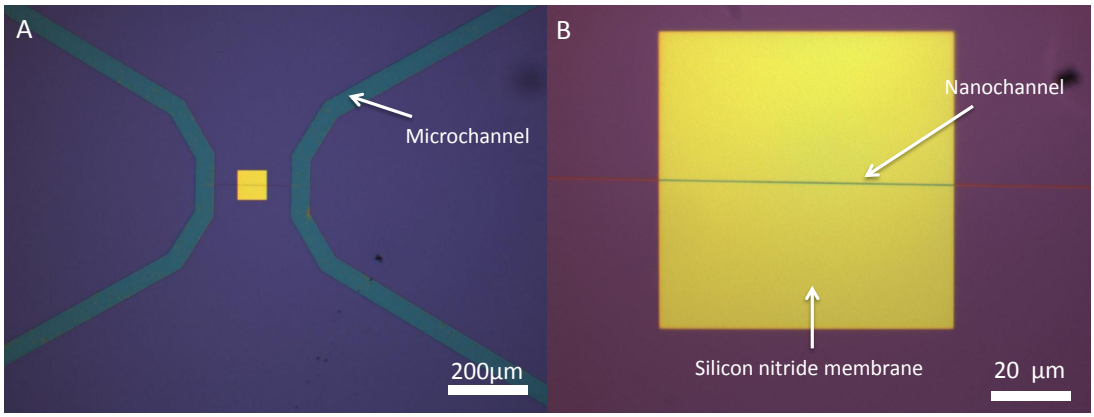

Figure 3–13: Optical microscope images of loading microchannels and nanochannel. A) Two u-shape loading microchannels are fabricated in the silicon nitride layer. B) nanochannel lying across the suspended membrane.

3.4.7 Nanopore fabrication

Nanopore is fabricated inside the nanochannel by electron ablation via TEM (introduced in chapter 2). By finely focusing electron beam on a nanometer scale spot, silicon nitride membrane is melted locally subsequently forming a nanopore. Inorganic dust (e.g. silicon and silicon nitride fragments) and carbon contamination (e.g. generic organics), which could potentially block the nanopore and fail the final bonding process, are serious issues for nano-structure (e.g. nanochannel, nanopore) fabrication.

In our process, the wafer is first coated with a layer of Shipley S1813 photoresist to prevent silicon dust contaminating the surface during the dicing process. The wafer is then diced into $5.95 \times 4.85\,\mathrm{mm}^2$ rectangular pieces. The corner of etch devices are also removed in order to fit our custom TEM sample holder. Photoresist as well as other organic residuals on each device are removed by piranha cleaning.

The nanochannel sample is then loaded in the TEM system ready for nanopore drilling. We first locate the silicon nitride membrane in the low magnification mode, then we find the center position along the 200 μm nanochannel at the magnification of 15 K×. Finally we go to the magnification of 500 k× or 600 k× and focus the beam inside the nanochannel. Given that the 160 nm deep nanochannel is etched across a 200 nm thick membrane, only 40 nm silicon nitride is left in the bottom region of the channel. While focusing the electron at the same region for several minutes, we would see a black ring suddenly appears on the fluorescent screen referring that a nanoscale pore is been drilled through.(Drifting of the beam is a serious issue during the pore fabrication process. Whenever drifting happens, we turn off the beam and wait for 30 min until the system stabilizes.) This newly drilled pore has a typical diameter of 2-3 nm. To fabricate nanopore with larger dimensions, electron beam is then focused on the edge of pore increasing the pore diameter until it reaches the desire value. To fabricate nanopore smaller than 2-3 nm, we spread the beam brighten the whole fluorescent screen. Instead of drilling a even larger pore, constant fluence of electrons of lower magnitude will activate and fluidize surrounding materials, shrinking the nanopore.

3.4.8 Sodium silicate bonding

As the final step of nanofluidics fabrication, bonding is a critical process, determining the success or failure of the whole fabrication. Conventional bonding protocols such as fusion bonding, which is performed at high temperature (e.g. 1000°C for fused silica, 600° for Pyrex [25, 26, 27, 28], will destroy the nanostructures on the suspended silicon nitride membrane. However, in 1997 H.Y Wang etc. [29] reported a technique of low temperature glass-to-glass bonding for microfabrication by utilizing sodium silicate as adhesion layer. By modifying

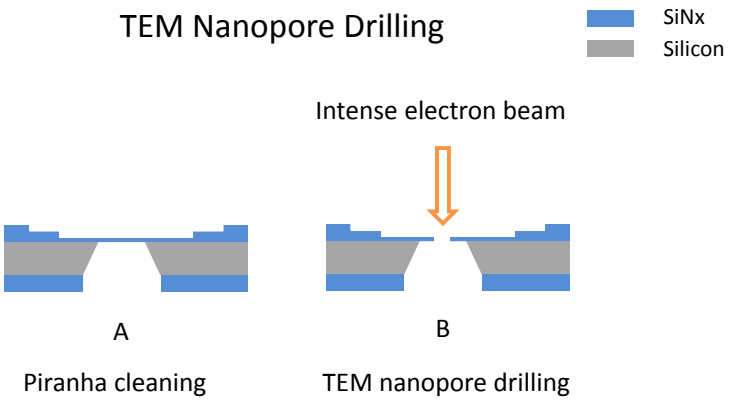

Figure 3–14: TEM nanopore drilling via electron ablation.

this process, we developed a special protocol for low temperature glass-to-silicon nitride bonding for nanofabrication.

Cleanness of the surface is a key parameter to the success of bonding, so the very first step of bonding process is surface cleaning. Nanopore-nanochannel chips and glass slides ($18 \times 18 \times 0.15\,\mathrm{mm}^3$ from Fisher Scientific) are placed in a custom teflon holder. Piranha solution (H_2SO_4:H_2O_2=3:1) is preheated to 90°C. Samples are then dipped in the piranha solution for at least 30 min to remove organic residuals. After cleaning, organic contaminations are removed and surface becomes extremely hydrophilic.

The second step of surface treatment is a modified RCA-1 cleaning process. The RCA clean, developed by Werner Kern in 1965 while working for the Radio Corporation of America (RCA), is a standard set of wafer cleaning steps involving three cleaning process:

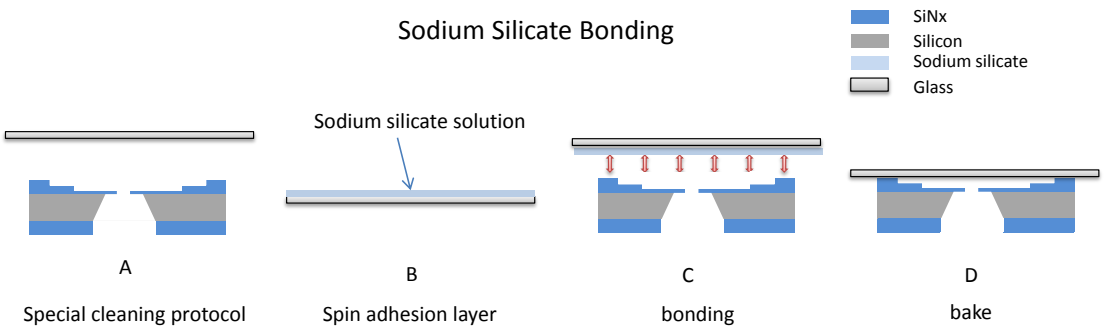

Figure 3–15: Diagrams of sodium silicate bonding process.

RCA-1: Removal of the organic contaminants;

RCA-2: Removal of thin oxide layer;

RCA-3: Removal of ionic contamination.

RCA-1 refers to organic cleaning process that is usually performed with a 1:1:5 solution of NH_4OH (ammonium hydroxide) + H_2O_2 (hydrogen peroxide) + H_2O (water) at 75°C. In the process, the mixture oxidizes the silicon surface and leaves a thin oxide layer (about 10 Angstrom) on the surface of the sample.

In our experiment, after piranha cleaning process, nanopore-nanochannel chips and coverslides are rinsed with DI water and then hydrolyzed in $NH_4OH/H_2O_2/H_2O$ (2:1:3) at 70°C for at least 20 min. Samples are rinsed with DI water and gently blow-dried with nitrogen right before bonding. Diluted sodium silicate solution (5.0 wt.%) is then spun on the glass cover at 4000 rpm for 15 s. After spinning, the treated coverslide surface is immediately brought in contact with the nanopore-nanochannel chip. Air bubbles trapped between the two surface are gently push out via tweezers. Finally, the bonded device is annealed at 90°C for 1 hour.

The bonding mechanism is believed to involve siloxane bond (Si-O-Si) formation between the sodium silicate layer and silicon nitride surfaces. Condensed Sodium silicate solution contains a high concentration of silicic acid ($Si(OH)_4$), formed through hydrolysis:

$SiO_2 + H_2O \rightleftharpoons Si(OH)_4$

At high PH (> 9), silicate ions are formed:

$Si(OH)_4 + OH^- \rightleftharpoons HSiO_3^- + 2H_2O$

$HSiO_3^- + OH^- \rightleftharpoons SiO_3^{2-} + H_2O$

Thus the cencentration of $Si(OH)_4$ is greatly lowered by conversion to ions at high pH. However when the concentrated sodium silicate solution is diluted and pH reduced, the concentration of hydroxyl ions (OH^-) is no longer sufficient to keep the silicate ions from being hydrolyzed to $Si(OH)_4$. Thus, a supersaturated solution of silicic acid with high reactivity is formed, which leads to its condensation-polymerization with any OH bearing surfaces until the supersaturation is relieved. The two hydrophilic surfaces are initially held together by hydrogen bonding and then joined by siloxane bond formation during the annealing process [29].

3.4.9 PDMS Molding

Given that the bonded nanopore-nanochannel chips have small device dimensions ($5.95 \times 4.85\,mm^2$, limited by the maximum sample size allowed by TEM sample holder), direct access of bulk fluidic reservoirs will be difficult. Consequently, we designed a PDMS medium layer that has millimetre scale fluidic channels to interface nanopore-nanochannel chip with a large scale glass slide ($75 \times 50 \times 1\,mm^3$) that has sand blasted holes on it.

PDMS (Polydimethylsiloxane) is a kind of silicon-based organic polymer. Being optically clear, non-toxic, non-flammable and chemically inert makes it an

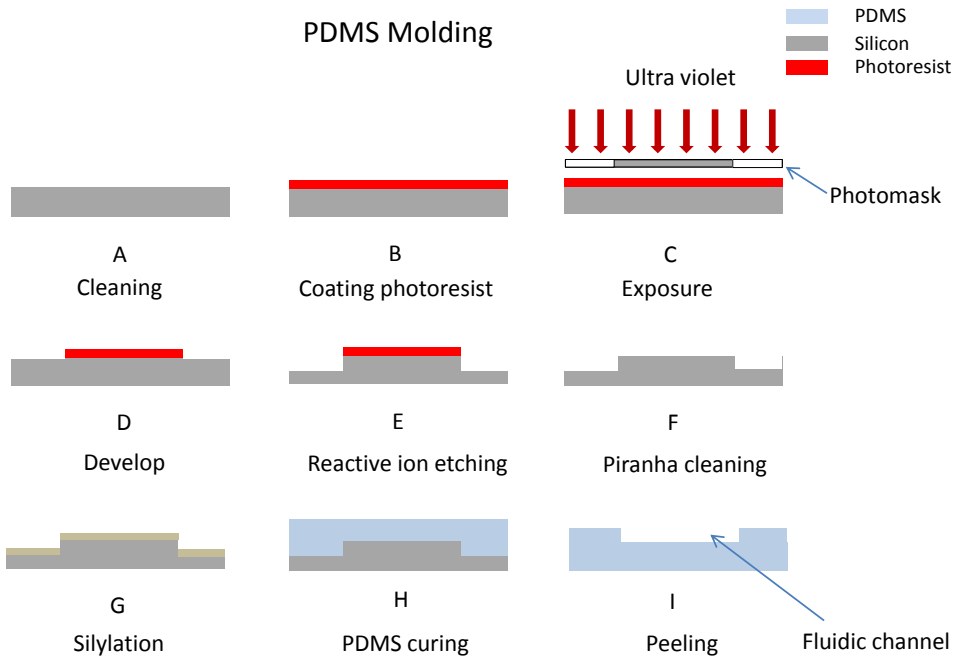

Figure 3–16: Diagrams of PDMS molding process.

ideal material for MEMS(Microelectromechanical systems), soft lithography and microfluidic device fabrication. In its raw form PDMS is a highly viscous flowing liquid. After mixing with curing agents and baking, it becomes structurally rigid. The curing agents act as branching points, helping form internal cross links that turn the PDMS into a flexible solid. Because of it's flowability before curing, PDMS are usually applied to a rigid mold that has microscale patterns. After curing process, PDMS becomes a replica of the mold that contains inverted structural information. Subsequently, possessing the advantages of simple molding process and reusable mold, PDMS molding technique are widely used for microfabrication nowadays.

In our process, PDMS molding process begins with mold fabrication. In order to fabricate a PDMS medium layer with millimetre fluidic channels, we need to make a mold that has inverted patterns. We first clean a 6 inch silicon wafer with acetone, IPA and DI water and then blow-dried with nitrogen gas. A layer of 1.4 μm thick Shipley S1813 photoresist is spun on the silicon substrate. After soft baking at 115 °C for 60 s, water is loaded in the contact aligner and patterned. Wafer is developed in MF319 developer for 45 s and then hard baked at 90 °C for 60 s.

Now that we have channel-patterned photoresist on silicon substrate. The surface is ready for silicon DRIE (deep reactive ion etching) process. In order to make a PDMS layer with concave channels, silicon mold must have convex structures, namely photoresist on the silicon wafer should only cover the fluidic channel regions that protects silicon from being etched. DRIE, which is originally devel-

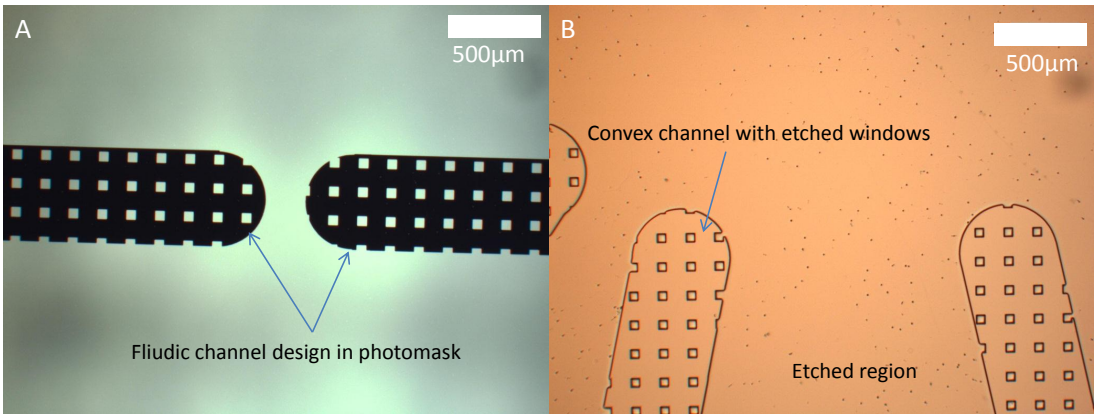

Figure 3–17: Optical microscope images of photomask and silicon substrate. A) Optical microscope image of the pattern design in the photomask for PDMS mold fabrication. B) Optical microscope image of silicon substrate after DRIE process. Special squares ($50 \times 50\,\mu m^2$) are etched in the silicon mold in order to produce posts in the PDMS fluidic channel preventing it from collapsing.

oped for microelectromechanical systems (MEMS), is a highly anisotropic etch

process used to create deep penetration, steep-sided holes and trenches in substrates. There are two main technologies for high-rate DRIE: Bosch and cryogenic. The Bosch process, developed by the German company Robert Bosch GmbH, alternates repeatedly between the etching mode and passivation mode to achieve nearly vertical structures. Each mode lasts for several seconds. The passivation layer (e.g. C_4F_8) protects the entire substrate from chemical attack and prevents etching. However, during the etching mode, the directional ions (mainly perpendicular to the wafer surface, accelerated by electromagnetic field) that bombard the substrate attack the passivation layer at the bottom of the trench. They collide with it and sputter it off, exposing the substrate to the chemical etchant. In cryogenic-DRIE process, wafer is chilled to -110 °C, so that the chemical reaction that produces isotropic etching is slowed down. However, ions that are accelerated by electromagnetic field continue bombarding upward-facing surfaces and etch them away creating vertical structures on wafer.

The silicon wafer is loaded in the Tegal SDE110 DRIE system, ready for Bosch process. The wafer is then cooled down to 0 °C with constant helium flow. The DRIE process begins with the passivation mode: 2 s 150 sccm C_4F_8 gas flow, and then shift to the etching mode: 4.5 s 300 sccm SF_6 gas flow. After repeating the two modes for 10 min, we have 30 μm deep convex channels on the silicon substrate (Figure 3-17 B).

In order to prevent PDMS sticking to the mold surface, silanization treatment is done by spreading 2% dimethyldichlorosinane solution ($Si(CH_2)_2Cl_2$) on the mold for 10 min.(Figure 3-16 G) Once the silicon mold is ready we need to apply PDMS on the mold surface and replicate the channel structure. The PDMS is prepared by mixing Sylgard 184 silicone elastomer base with curing agent (10:1).

Stirring is necessary for an uniform mix. The mixture is then poured on the silicon mold and degassed in desiccator until all air bubbles are removed (takes around 15 min). The sample is then placed in an oven and baked at 70 °C for 1 h.(Figure 3-16 H) Fully cured PDMS layer is removed from the oven and then separated from one side of the mold using a blade.(Figure 3-16 I)

3.4.10 PDMS Bonding

As mentioned in the previous subsection, PDMS layer only serves as a medium layer for glass slide and nanopore-nanochannel chip. To connect fluidic channel in the PDMS layer with fluidic reservoirs in the nanopore-nanochannel chip, holes are punched through in the PDMS sample according to the position of reservoirs. (Figure 3-18 A) The PDMS sample is firstly bonded to a 75×50×1 mm(2.95 x 1.96 x .040") glass slide (the surface with fluidic channels is bonded to glass slide). The nanopore-nanochannel chip is then bonded to the PDMS layer (the surface without fliudic channels is bonded to nanopore-nanochannel chip). Thus, the fluidic reservoirs are connected with the holes on the glass slide via fluidic channels and pre-punched holes on the PDMS layer.(Figure 3-18 C)

The glass-to-PDMS and silicon nitride-to-PDMS surface is bonded via oxygen plasma. The mechanism of oxygen plasma bonding is that in general PDMS material comprises of repeated units of -O-Si(CH_3)$_2$, this group will develop silanol group (Si-OH) at the expense of methyl groups(-CH_3) while exposed in oxygen plasma [30]. The oxidation of the glass or silicon nitride surface layer increases the concentration of hydroxyl groups (-OH), thus increase the number of silanol group since the substrates containing activated silicon molecules. When two activated surfaces are brought into contact, these silanol groups condense with those on

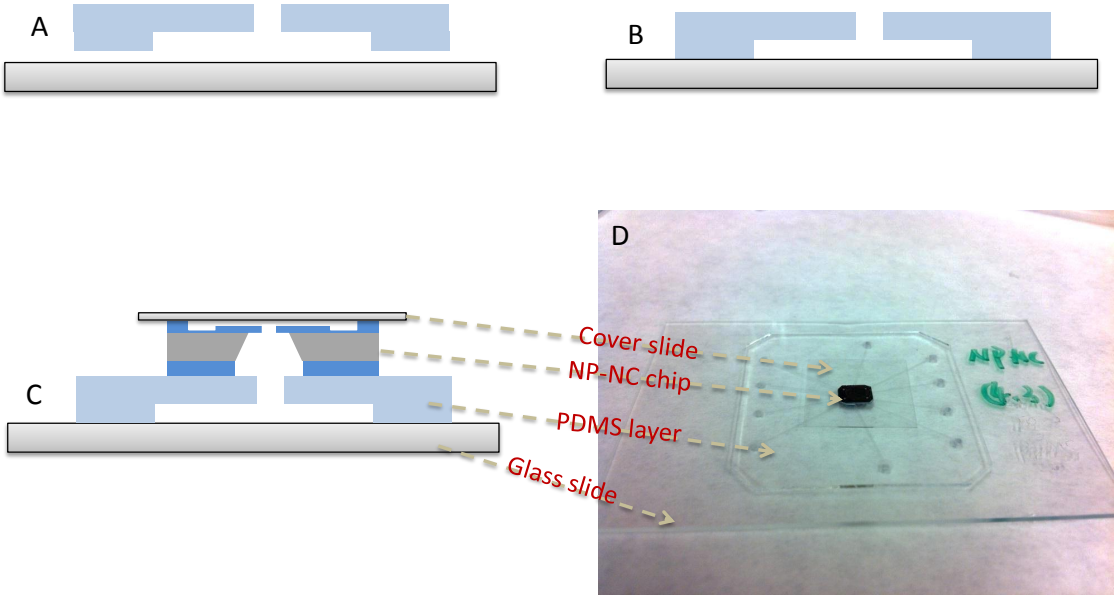

Figure 3–18: Diragrams of PDMS bonding process.

another surface. For both PDMS-to-glass bonding and PDMS-to-silicon nitride bonding, these reactions yield Si-O-Si bonds after loss of a water molecule [31, 32].

To ensure the bonding quality, PDMS samples and glass slides are cleaned with acetone, IPA and DI water. Samples are then placed in the quartz chamber of PVA TePla oxygen plasma system. Vacumm pump is on and the chamber pressure drops down to 0.2 mbar. Once the vacuum is ready, oxygen flow is turned on, pressure will be stabilized at around 1 mbar after a few seconds. Plasma is then activated and maintained for 30 s at the power of 70 W. After surface activation, vacuum pump and oxygen flow is turned off, and the PDMS surface is immediately brought into contact with glass slide.(Figure 3-18 B) Pressure are applied via hands to remove trapped air bubbles as well as strengthen bonding. Samples are then placed in an oven heating at 70 °C for 1 h to further increase bond strength. Once the PDMS layer is bonded with glass slide, nanopore-nanochannel chips

are bonded to the PDMS layer following the same protocol.(Figure 3-18 C) The assembled view of nanopore-nanochannel chip, PDMS layer and glass slide after bonding is shown in figure 3-18 D.

3.5 Device characterization via TEM

Nanopore-nanochannel samples are characterized via TEM before sodium silicate bonding . A 200 kV field emission gun TEM from JEOL, JEL-2100F, was employed to carry out these experiments. A custom sample holder is used for loading nanopore-nanochannel chips to the TEM system. Emission current is set between $170 \sim 185\,\mu$A. A fluence of $10^5\ e \cdot nm^{-2}$ or lower was used for imaging.

Membrane contamination

Two images of nanochannel crossing the 200 nm thick silicon nitride membrane are shown in figure 3-19. Contaminations (mostly carbon residue) are found on the membrane window, which was not cleaned with piranha solution (Figure

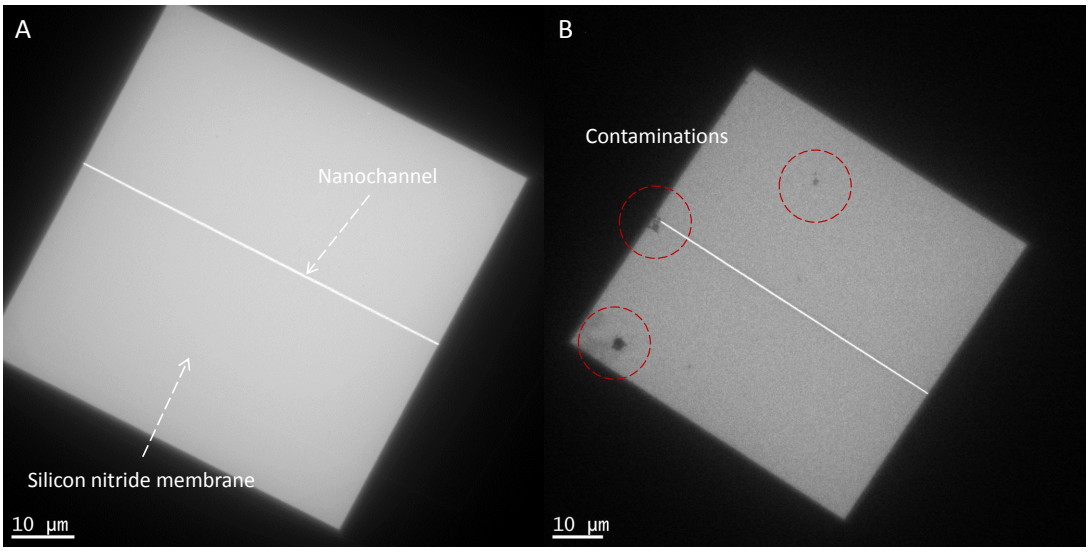

Figure 3–19: Nanochannel crossing the free standing silicon nitride membrane. A) after piranha cleaning process. B) before piranha cleaning process. Images are taken at low MAG mode.

3-19 B). After the cleaning process organic contamination is removed, a clean free standing membrane is shown in figure 3-19 A.

Nanochannels

Nanochannels are carefully inspected, before drilling a nanopore inside the channel. Defects, due to the RIE process, are found in some of our samples. As shown in figure 3-20 A, because of excessive etching a nanochannel is totally etched through the silicon nitride membrane during the RIE process, thus splitting the membrane in half from the center (no material left inside the channel). As the etching time reduced material located at the edge of the nanochannel is preserved

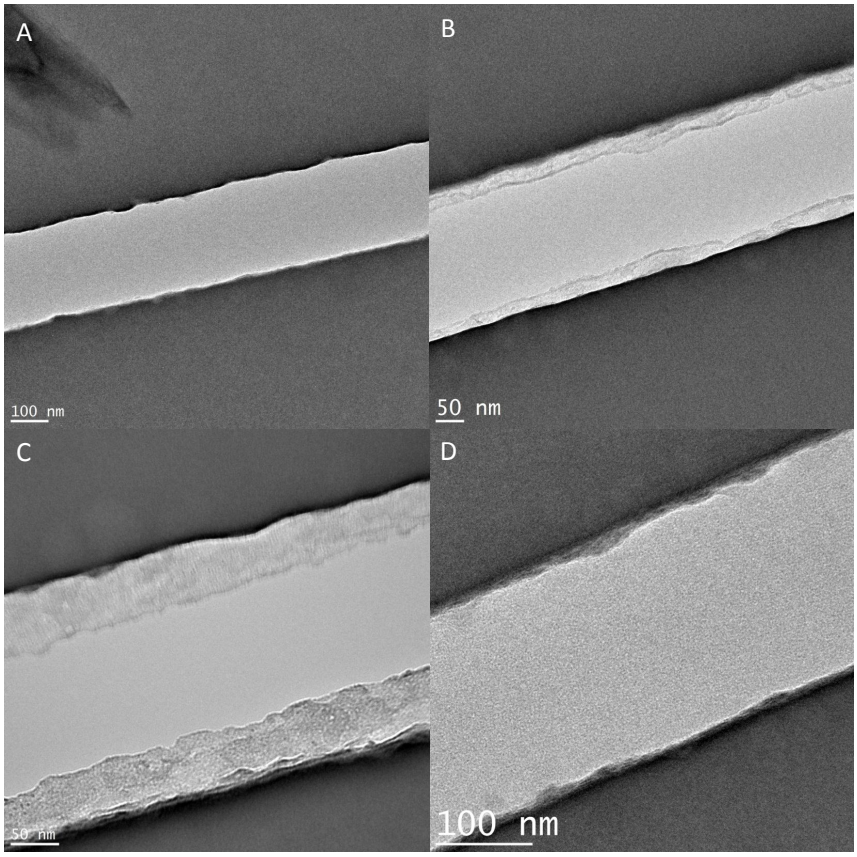

Figure 3–20: Nanochannels on the silicon nitride membrane. A) channel totally etched through. B),C) channels partially etched through. D) a functional nanochannel with silicon nitride material preserved at the channel bottom.

(less ions bump to the edge due to the shadow effect of vertical channel wall during RIE process), only the channel center is etched through.(figure 3-20 B and C) Further decreasing of etching time results in a non-destructive concave nanochannel on the membrane. A 40 nm thick layer of silicon nitride membrane is preserved in the nanochannel.(figure 3-20 D)

Silicon nitride membrane

As mentioned in section 3.4.2, silicon nitride membrane are deposited via PECVD on silicon substrate. High resolution TEM image of ultra thin silicon nitride layer, located at the edge of the channel, shows the amorphous molecular structure of silicon nitride membrane, no crystallization is observed.(Figure 3-21)

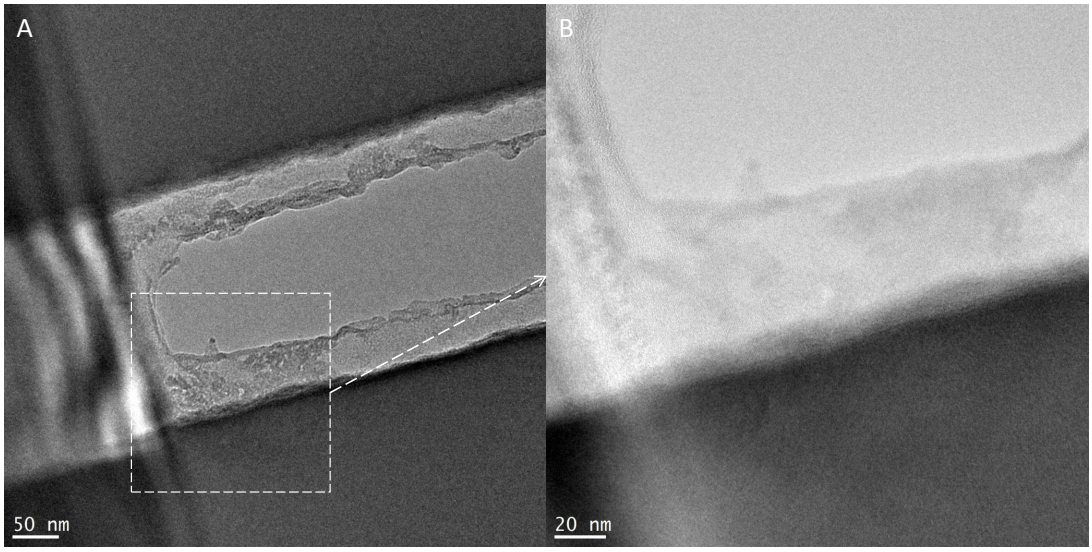

Figure 3–21: Amorphous silicon nitride layer. A) untra thin silicon nitride membrane inside nanochannel. B) high resolution image of the membrane structure.

Nanopore in nanochannel

As long as the nanochannel remains functional (no defects on the membrane of the channel bottom), nanopores of various sizes are drilled on the bottom

thin membrane via TEM. Figure 3-22 shows the image of three different sized nanopores drilled inside channel.

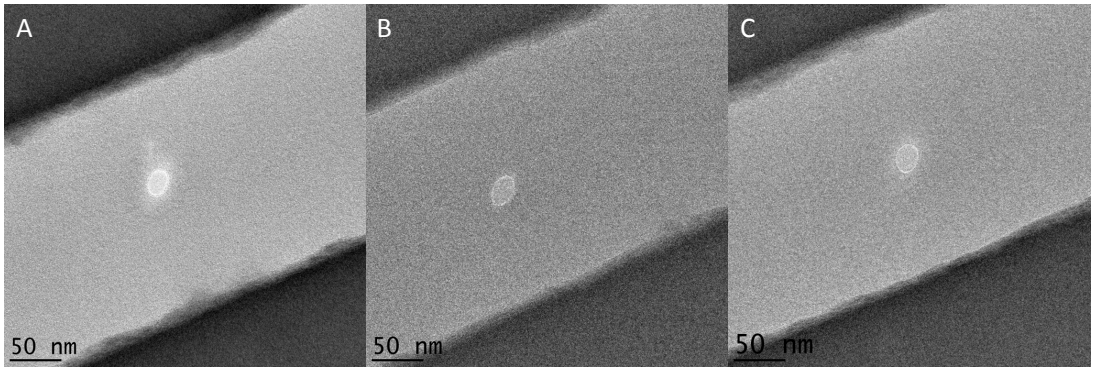

Figure 3–22: TEM images of three different sized nanopores fabriated inside the nanochannel.

Over all structure

The relative positions of the loading microchannels, silicon nitride window, nanochannel and nanopore are shown in the figure 3-23. The nanochannel that is etched across the silicon nitride membrane window is interfaced to two loading microchannels at its ends. The nanochannel also contains a 21 nm pore embedded in the bottom membrane at the center of the channel.

3.6 Experimental setup

3.6.1 Buffer preparation

λ-DNA molecules are stained with YOYO-1 ($C_{49}H_{58}I_4N_6O_2$) fluorescent die at the ratio of 10: 1, DNA base pairs to die molecules, for visualization. The stoke DNA with an original concentration of 500 μg/mL was diluted 10 times with TE buffer (10 mM Tris (tris(hydroxymethyl)aminomethane)/ 1 mM ETDA (ethylenediaminetetraacetic acid)). YOYO-1 with an original concentration of 1 M was diluted to 100 μM then vortexed. TE buffer, diluted DNA molecules and

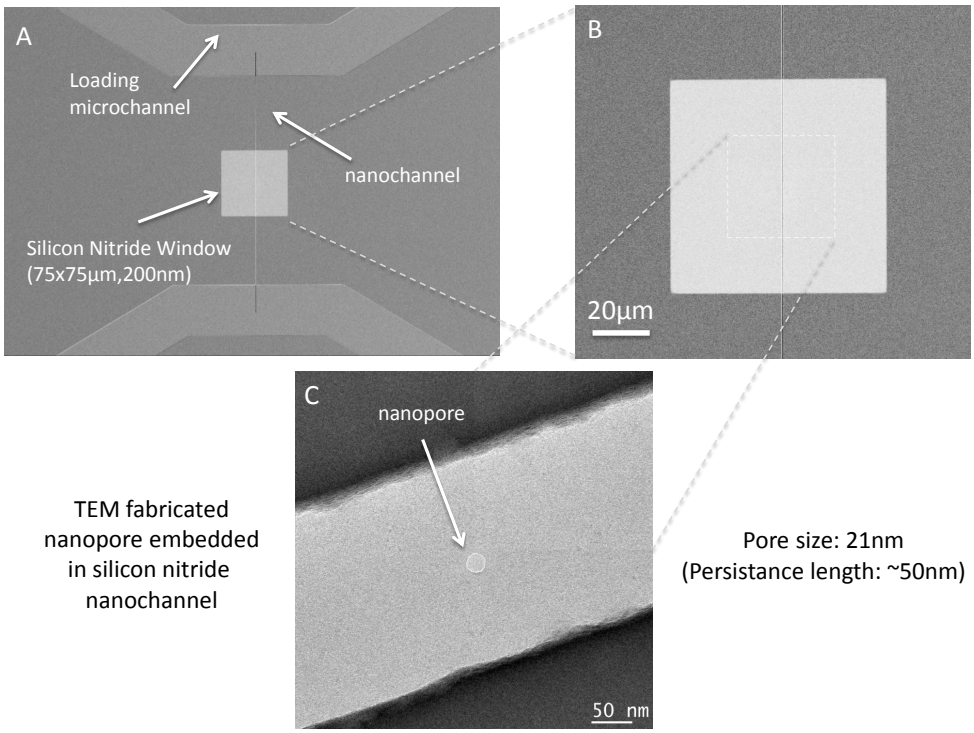

Figure 3–23: TEM and SEM images showing the relative positions of the nanopore-nanochannel structure.

YOYO-1 were mixed at the ratio of 157:3:40 to ensure a 10:1 staining ratio. Buffer was mixed gently (avoiding damaging DNA molecules) by repeatedly drawing it from the bottom and releasing it from the top via a large orifice pipette tip. 2% of BME (2-mercaptoethanol) was added to suppress bleaching and photoknicking of DNA.

3.6.2 Nanopore-nanochannel fluidic cell

During experiments, the bonded chip was sealed by an aluminum retaining ring to a plastic (PMMA) fluidic cell (figure 3-24). The cell is anchored to the positioning stage of a microscope. The fludic cell was designed to provide pressure

access, optical access and the possibility of carrying out electric measurements. Reservoirs in the chuck are connected with the fluidic reservoirs at the bottom of nanopore-nanochannel chip via PDMS medium layer. Buffer is pipetted in the cell reservoirs, and then pushed in the PDMS fluidic channel, and eventually pushed in to the nanopore-nanochannel chip via pressure (or capillary action for the initial wetting process)(figure 3-25).

3.6.3 Measuring technique

For florescent imaging, a Nikon Eclipse Ti inverted microscope was used. Nikon Plan Apo VC 100 × oil immersion objective lens was mounted for magnification. The fluidic cell was attained the positioning stage controlled by a Prior Proscan III. Illumination was provided by a X-Cite Series 120 lamp, focused with a condenser-aperture through a filter. Absorption peak of YOYO-1 is at 491 nm, while emission peak is at 509 nm. The shutter was controlled by Lambda SC controller. Signal was acquired by an Andor iXon digital camera with a cooled (-80°C) electron-mulitiplying charge-coupled device (EMCCD). NIS Elements software was used for data acquisition.

3.7 Results and discussion

3.7.1 DNA in microchannel

In our experiments, we have successfully pushed DNA molecules into nanopore-nanochannel chips via pressure. Figure 3-27 shows the stained λ-DNA molecule entering microchannel through the fluidic reservoir on chip. Due to the unbalanced pressure and concentration gradient, DNA molecules move into microchannel rapidly.

The following figure clearly illustrate the effect of pressure in micro/nanofluidic system. Figure 3-28 shows DNA molecules moving inside the nanochannel under

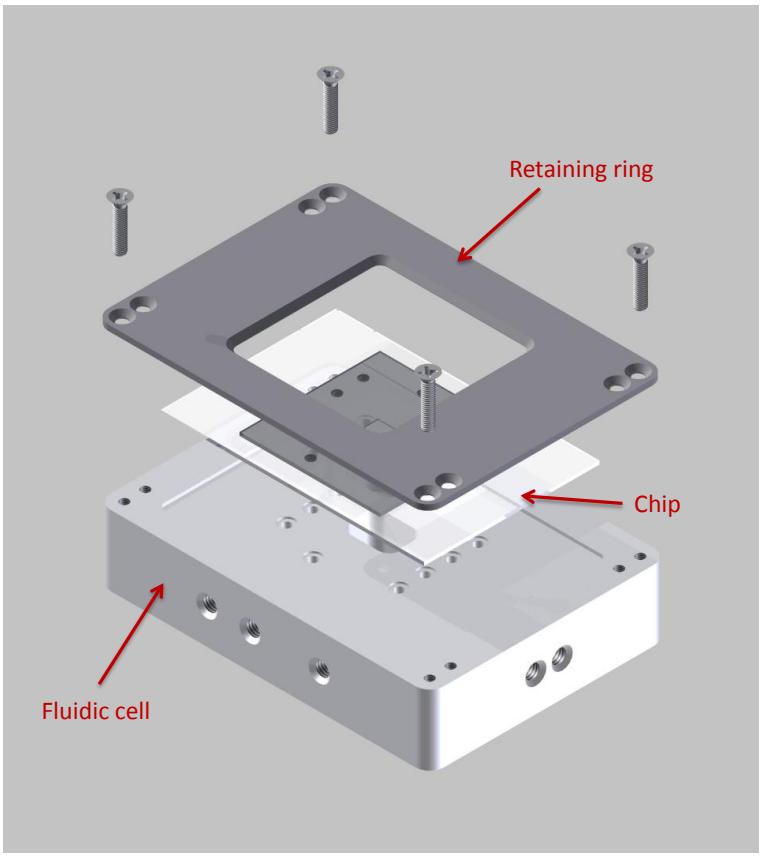

Figure 3–24: Schematic view of disassembled experimental setup, cell, chip and retaining ring.

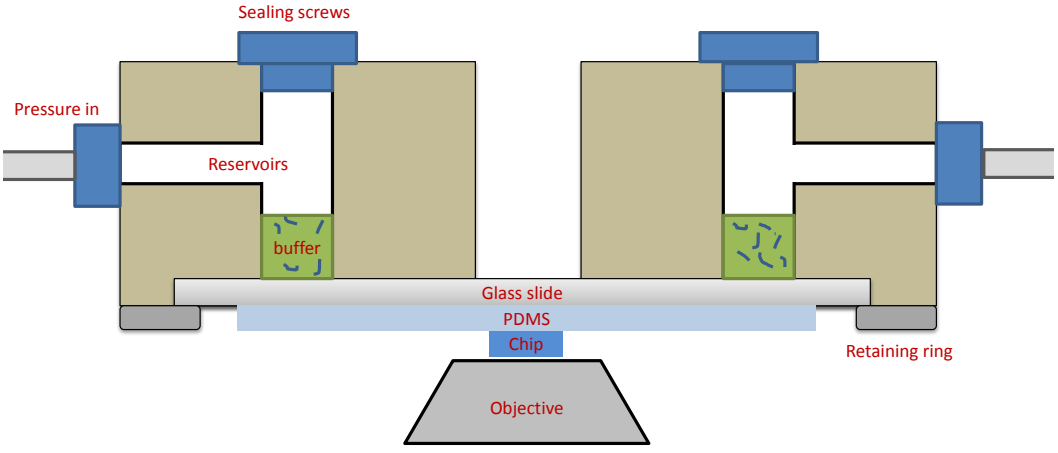

Figure 3–25: schematic diagram of DNA buffer entering nanopore-nanochannel chip.

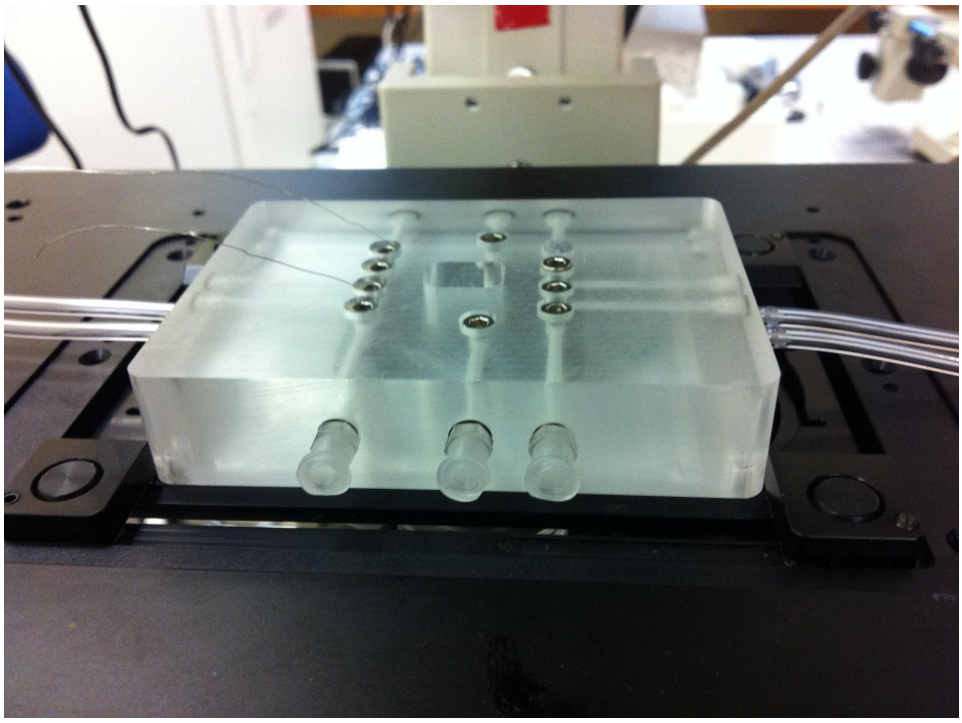

Figure 3–26: Fluidic cell mounted on the positioning stage of inverted microscope.

different pressure. As shown in figure 3-28 A, only a pressure of $\sim$ 50mbar is applied to the system, DNA molecules move at a relatively slow speed ($\sim 3\,\mu$m/s). However, when the pressure increased by 10 times ($\sim$500mbar), DNA molecules move at higher speed ($\sim 30\,\mu$m/s) and are also stretched into a longer conformation. This result is consistent with the Hagen-Poiseuille law.

$$\Delta p = R_{hyd} Q \tag{3.22}$$

When Δp increase by 10 times, the flux Q (given by $v \cdot S$, v is the flow rate, S is the channel cross-sectional area) increases by 10 times. Given that channel dimension and hydraulic resistance is constant, flow rate v will increase by 10 times.

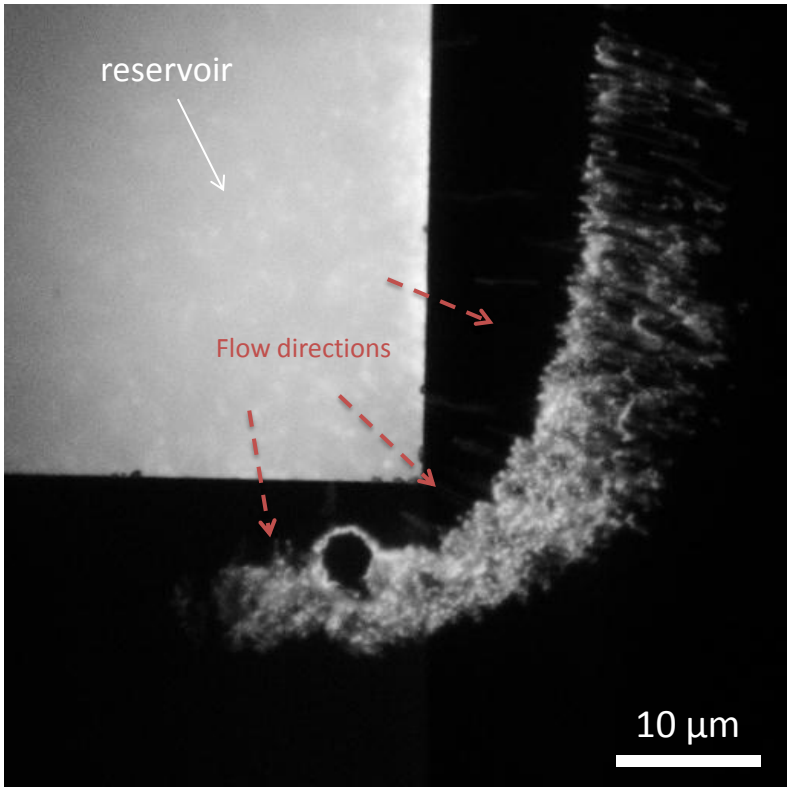

Figure 3–27: DNA molecules moving from reservoirs to the microchannel driven by pressure.

3.7.2 DNA in nanochannel

DNA molecules are then pushed into the nanochannel via higher pressure (∼700mbar). Figure 3-29 A shows a λ-DNA molecule inside the nanochannel, DNA molecule is stretched to around 5 μm due to the low dimensional confinement. Picture B, shows the position of a labeled DNA molecule inside nanochannel fluctuating over time.

3.7.3 Discussion

From the previous result, we know that DNA molecules have been successfully loaded into the integrated nanopore-nanochannel system, sodium silicate

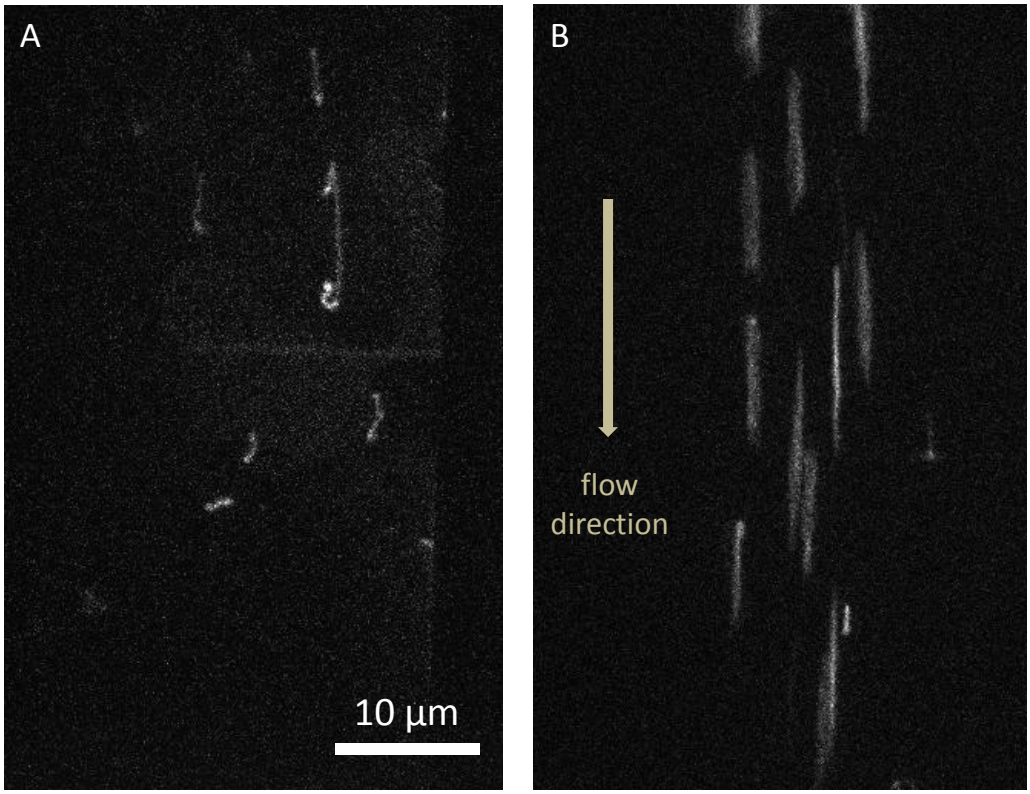

Figure 3–28: DNA in microchannel. A) a low pressure ($\sim 50\,\mathrm{mbar}$) is applied across the microchannel, DNA molecules move at a low speed ($\sim 3\,\mu\mathrm{m/s}$). B) a relatively high pressure ($\sim 500\,\mathrm{mbar}$) is applied across the microchannel, DNA molecules move at $\sim 30\,\mu\mathrm{m/s}$.

bonded silicon nitride microchannel and nanochannel are proven to be functional. Even though we haven't collected enough data of the stained λ-DNA molecules interacting with the different sized naonopores embedded inside nanochannels, predictions can be made:

For nanopore larger than DNA persistence length (> P), while being pushed into the nanochannel, stained DNA molecules will be moving from one end of

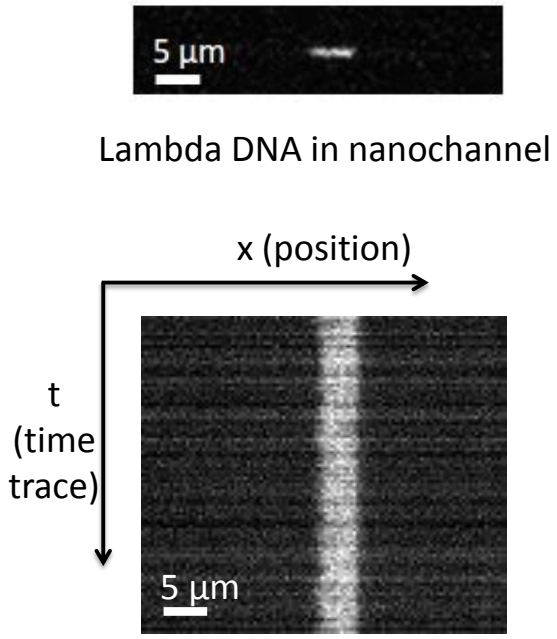

Figure 3–29: DNA molecules in nanochannel. λ-DNA molecule is pushed in the nanochannel via pressure, and it stretches to around 5 nm under the nanochannel (160 nm $\times$ 200 nm) confinement.

the nanochannel to the other. When is reaches the center position, the molecular length detected by the CCD camera decreases with time, and finally disappears. Indicating that DNA molecules have successfully translocated through the nanopore.

For nanopore smaller than DNA persistence length ($<$ P), stained DNA molecules will move along the nanochannel instead of going into the pore region. Molecular length determined by fluorescent signals will not change significantly.

CHAPTER 4
Conclusions

A classic nanopore setup based on a simple electrochemical system is used for the single dsDNA molecule detection. Nanopores are successfully fabricated via focusing electron beam on thin silicon nitride film utilizing a TEM. An stable open pore current in the order of several nA is acquired while applying a voltage of $100\,mV$ across a nanopore. Coating a thin layer of PDMS on the supporting chip, has been proven as an effective way of reducing electric noise at low frequency region. Multilevel structures are observed in electric blockade signal, showing that different conformations of DNA molecules passing a nanopore are detected, referring to different states of molecular folding structures.

A novel device that combines the advantages of both nanopore detectors and nanochannel devices, is presented. Device feasibility is proven via simple theoretic analysis. The integrated micro/nanofuidic system is successfully fabricated by combining various of micro/nanofabrication techniques, such as photolithography, reactive ion etching, e-beam lithography, TEM nanopore drilling and so on. We have also developed a special protocol for low temperature bonding of silicon nitride to glass surface via diluted sodium silicate as adhesion layer for nanofluidic system. DNA molecules are successfully pushed into the microchannel and nanochannel via pressure.

Future work will focus on analysing the interaction between DNA molecules and varying sized solid state nanopores as well as pushing the limit of DNA electric sensing by shrinking the pore size in the nanopore-nanochannel system.

References

[1] W Gilbert and A Maxam. The nucleotide sequence of the lac operator. *Proceedings of the National Academy of Sciences of the United States of America*, 70(12):3581–4, December 1973.

[2] F Sanger and S Nicklen. DNA sequencing with chain-terminating. 74(12):5463–5467, 1977.

[3] J Dondorp. The thousand-dollar genome : an ethical exploration. *Ethics*, 2010.

[4] J Watson and M Egholm. The thousand-dollar genome. *Molecular Biology*, 2007.

[5] W D David and A Mark. Nanopores and nucleic acids: prospects for ultrarapid sequencing. *Trends in Biotechnology*, 18(4):147 – 151, 2000.

[6] J J Kasianowicz, E Brandin, D Branton, and D W Deamer. Characterization of individual polynucleotide molecules using a membranechannel. *Proceedings of the National Academy of Sciences*, 93(24):13770–13773, 1996.

[7] C Dekker. Solid-state nanopores. *Nature nanotechnology*, 2(4):209–15, April 2007.

[8] J Li, D Stein, C McMullan, D Branton, M J Aziz, and J a Golovchenko. Ion-beam sculpting at nanometre length scales. *Nature*, 412(6843):166–9, July 2001.

[9] A J Storm, J H Chen, X S Ling, H W Zandbergen, and C Dekker. Fabrication of solid-state nanopores with single-nanometre precision. *Nature materials*, 2(8):537–40, August 2003.

[10] G M Whitesides. The origins and the future of microfluidics. *Nature*, 442(7101):368–73, July 2006.

[11] F K Balagadd, L You, C L Hansen, F H Arnold, and S R Quake. Long-term monitoring of bacteria undergoing programmed population control in a microchemostat. *Science*, 309(5731):137–140, 2005.

[12] D R Gossett, W M Weaver, A J Mach, S C Hur, H T K Tse, W Lee, H Amini, and Dino Di Carlo. Label-free cell separation and sorting in microfluidic systems. *Analytical and bioanalytical chemistry*, 397(8):3249–67, August 2010.

[13] D B Weibel, M Kruithof, S Potenta, and S K Sia. Torque-actuated valves for microfluidics. *Analytical*, 77(15):4726–4733, 2005.

[14] F Brochard-Wyart, T Tanaka, N Borghi, and P-G De Gennes. Semiflexible polymers confined in soft tubes. *Langmuir The Acs Journal Of Surfaces And Colloids*, 21(9):4144–4148, 2005.

[15] T Odijk. The statistics and dynamics of confined or entangled stiff polymers. *Macromolecules*, 16(8):1340–1344, 1983.

[16] V Tabard-Cossa, D Trivedi, M Wiggin, N N Jetha, and A Marziali. Noise analysis and reduction in solid-state nanopores. *Nanotechnology*, 18(30):305505, 2007.

[17] J Li, M Gershow, D Stein, E Brandin, and J A Golovchenko. DNA molecules and configurations in a solid-state nanopore microscope. *Nature materials*, 2(9):611–5, September 2003.

[18] R M M Smeets, U F Keyser, D Krapf, M-Y Wu, N H Dekker, and C Dekker. Salt dependence of ion transport and DNA translocation through solid-state nanopores. *Nano letters*, 6(1):89–95, January 2006.

[19] W Reisner, K J Morton, R Riehn, Y M Wang, Z Yu, M Rosen, J C Sturm, S Y Chou, E Frey, and R H Austin. Statics and dynamics of single dna molecules confined in nanochannels. *Phys. Rev. Lett.*, 94:196101, May 2005.

[20] H Bruus. *Theoretical Microfluidics (Oxford Master Series in Physics)*. Oxford University Press, USA, November 2007.

[21] R Doering and Y Nishi. *Handbook of semiconductor manufacturing technology*. CRC Press, 2 edition, July 2008.

[22] Comparison vertical vs. horizontal furnaces, June 2009.

[23] C Cheung, K Luo, D Li, D Ngo, L Dang, J Uyeda, J Wang, and M Barsky. Silicon nitride surface preparation to prevent photoresist blister defects. *GaAs Manuf. Technol. Conf. Dig.*, 77:14, 2005.

[24] Wikipedia. Etching (microfabrication) — Wikipedia, the free encyclopedia, 2012. [Online; accessed 01-May-2012].

[25] T Tsukahara, Mawatari, A Hibara, and T Kitamori. Development of a pressure-driven nanofluidic control system and its application to an enzymatic reaction. *Analytical and Bioanalytical Chemistry*, 391:2745–2752, 2008. 10.1007/s00216-008-2198-2.

[26] P Mao and J Han. Fabrication and characterization of 20 nm planar nanofluidic channels by glass-glass and glass-silicon bonding. *Lab Chip*, 5:837–844, 2005.

[27] J S Mellors, V Gorbounov, R S Ramsey, and J M Ramsey. Fully integrated glass microfluidic device for performing high-efficiency capillary electrophoresis and electrospray ionization mass spectrometry. *Analytical Chemistry*, 80(18):6881–6887, 2008.

[28] Y Xu, K Sato, K Mawatari, T Konno, K Jang, K Ishihara, and T Kitamori. A microfluidic hydrogel capable of cell preservation without perfusion culture under cell-based assay conditions. *Advanced Materials*, 22(28):3017–3021, 2010.

[29] H Y Wang, R S Foote, S C Jacobson, J H Schneibel, and J M Ramsey. Low temperature bonding for microfabrication of chemical analysis devices. *Sensors and Actuators B: Chemical*, 45(3):199 – 207, 1997.

[30] S Bhattacharya, A Datta, J M Berg, and S Gangopadhyay. Studies on Surface Wettability of Poly (Dimethyl) Siloxane (PDMS) and Glass Under Oxygen-Plasma Treatment and Correlation With Bond Strength. 14(3):590–597, 2005.

[31] H Hillborg and U W Gedde. Hydrophobicity recovery of polydimethylsiloxane after exposure to corona discharges. *Polymer*, 39(10):1991 – 1998, 1998.

[32] M L Chabinyc, D T Chiu, J C McDonald, A D Stroock, J F Christian, A M Karger, and G M Whitesides. An integrated fluorescence detection system in poly(dimethylsiloxane) for microfluidic applications. *Analytical Chemistry*, 73(18):4491–4498, 2001.